.

Dynamical 3-Space: A Review

Reginald T. Cahill
School of Chemistry, Physics and Earth Sciences,
Flinders University, Adelaide 5001, Australia

For some 100 years physics has modelled space and time via the *space-time* concept, with space being merely an observer dependent perspective effect of that spacetime - space itself had no observer independent existence - it had no ontological status, and it certainly had no dynamical description. In recent years this has all changed. In 2002 it was discovered that a dynamical 3-space had been detected many times, including the Michelson-Morley 1887 light-speed anisotropy experiment. Here we review the dynamics of this 3-space, tracing its evolution from that of an emergent phenomena in the information-theoretic *Process Physics* to the phenomenological description in terms of a velocity field describing the relative internal motion of the structured 3-space. The new physics of the dynamical 3-space is extensively tested against experimental and astronomical observations, including the necessary generalisation of the Maxwell, Schrödinger and Dirac equations, leading to a derivation and explanation of gravity as a refraction effect of the quantum matter waves. Phenomena now explainable include the bore hole anomaly, the systematics of black hole masses, the flat rotation curves of spiral galaxies, gravitational light bending and lensing, and the supernova and Gamma-Ray Bursts magnitude-redshift data, for the dynamical 3-space possesses a Hubble expanding 3-space solution. Most importantly none of these phenomena now require dark matter nor dark energy. The flat and curved spacetime formalism is derived from the new physics, so explaining the apparent many successes of those formalisms, but which have now proven to be ontologically and experimentally flawed.

Contents

1 Introduction

We review here some of the new physics emerging from the discovery that there exists a dynamical 3-space. This discovery changes all of physics. While at a deeper level this emerges from the information-theoretic Process Physics [1, 4, 5, 6, 7, 8, 9] here we focus on the phenomenological description of this 3-space in terms of the velocity field that describes the internal dynamics of this structured 3-space. It is straightforward to construct the minimal dynamics for this 3-space, and it involves two constants: G - Newton's gravitational constant, and α - the fine structure constant. G quantifies the effect of matter upon the flowing 3-space, while α describes the self-interaction of the 3-space. Bore hole experiments and black hole astronomical observations give the value of α as the fine structure constant to within observational errors. A major development is that the Newtonian theory of gravity [10] is fundamentally flawed - that even in the non-relativistic limit it fails to correctly model numerous gravitational phenomena. So Newton's theory of gravity is far from being 'universal'. The Hilbert-Einstein theory of gravity (General Relativity - GR), with gravity being a curved spacetime effect, was based on the assumption that Newtonian gravity was valid in the non-relativistic limit. The ongoing effort to save GR against numerous disagreements with experiment and observation lead to the invention first of 'dark matter' and then 'dark energy'. These effects are no longer required in the new physics. The 3-space velocity field has been directly detected in at least eight experiments including the Michelson-Morley experiment [2] of 1887, but most impressively by the superb experiment by Miller in 1925/1926 [3]. The Miller experiment was one of the great physics experiments of the 20th century, but has been totally neglected by mainstream physics. All of these experiments detected the dynamical 3-space by means of the light speed anisotropy - that the speed of light is different in different directions, and the anisotropy is very large, namely some 1 part in a 1000. The existence of this 3-space as a detectable phenomenon implies that a generalisation of all the fundamental theories of physics be carried out. The generalisation of the Maxwell equations leads to a simple explanation for gravitational light bending and lensing effects, the generalisation of the Schrödinger equation leads to the first derivation of gravity - as a refraction effect of the quantum matter waves by the time dependence and inhomogeneities of the 3-space, leading as well to a derivation of the equivalence principle. This generalised Schrödinger equation also explains the Lense-Thirring effect as being caused by vorticity in the flowing 3-space. This effect is being studied by the Gravity Probe B (GP-B) gyroscope precession experiment. The generalisation of the Dirac equation to take account of the interaction of the spinor with the

dynamical 3-space results in the derivation of the curved spacetime formalism for the quantum matter geodesics, but without reference to the GR equations for the induced spacetime metric. What emerges from this derivation is that the spacetime is purely a mathematical construct - it has no ontological status. That discovery completely overturns the paradigm of 20th century physics. The dynamical equation for the 3-space has black hole solutions with properties very different from the putative black holes of GR, leading to the verified prediction for the masses of the minimal black holes in spherical star systems. That same dynamics has an expanding 3-space solution - the Hubble effect for the universe. That solution has the expansion mainly determined by space itself. This expansion gives a extremely good account of the supernovae/Gamma-Ray Burst redshift data without the notion of 'dark energy' or an accelerating universe. This review focuses on the phenomenological modelling of the 3-space dynamics and its experimental checking. Earlier reviews are available in [1](2005) and [4](2003). Page limitations mean that some developments have not been discussed herein.

2 Dynamics of 3-Space

At a deeper level an information-theoretic approach to modelling reality, *Process Physics* [1], leads to an emergent structured quantum foam 'space' which is 3-dimensional and dynamic, but where the 3-dimensionality is only approximate, in that if we ignore non-trivial topological aspects of the space, then it may be embedded in a 3-dimensional geometrical manifold. Here the space is a real existent discrete but fractal network of relationships or connectivities, but the embedding space is purely a mathematical way of characterising the gross 3-dimensionality of the network. This is illustrated in Fig.1. Embedding the network in the embedding space is very arbitrary; we could equally well rotate the embedding or use an embedding that has the network translated or translating. These general requirements then dictate the minimal dynamics for the actual network, at a phenomenological level. To see this we assume at a coarse grained level that the dynamical patterns within the network may be described by a velocity field $\mathbf{v}(\mathbf{r}, t)$, where $\mathbf{r}$ is the location of a small region in the network according to some arbitrary embedding. The 3-space velocity field has been observed in at least 8 experiments [2, 3, 16, 17, 18, 19, 20, 21, 22, 23, 24]. For simplicity we assume here that the global topology of the network is not significant for the local dynamics, and so we embed in an E^3, although a generalisation to an embedding in S^3 is straightforward and might be relevant to cosmology. The minimal dynamics is then obtained by writing down the lowest-order zero-rank tensors, of dimension

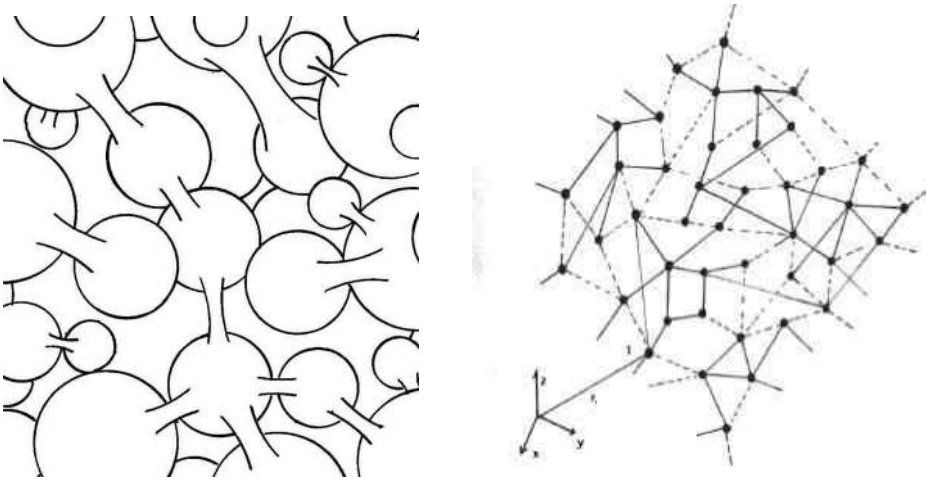

Figure 1: This is an iconic representation of how a quantum foam dynamical network (left), see [1] for details of the Quantum Homotopic Field Theory, has its inherent approximate 3-dimensional connectivity displayed by an embedding in a mathematical space, such as an E^3 or an S^3 as shown on the right. The embedding space is not real; it is purely a mathematical artifact. Nevertheless this embeddability helps determine the minimal dynamics for the network, as in (1). The dynamical space is not an ether model, as the embedding space does not exist.

$1/t^2$, that are invariant under translation and rotation, giving

$$\nabla.\left(\frac{\partial \mathbf{v}}{\partial t}+(\mathbf{v}.\nabla)\mathbf{v}\right)+\frac{\alpha}{8}(trD)^2+\frac{\beta}{8}tr(D^2)=-4\pi G\rho;\quad D_{ij}=\frac{1}{2}\left(\frac{\partial v_i}{\partial x_j}+\frac{\partial v_j}{\partial x_i}\right) \tag{1}$$

where $\rho(\mathbf{r},t)$ is the matter and EM energy densities expressed as an effective matter density. The embedding space coordinates provide a coordinate system or frame of reference that is convenient to describing the velocity field, but which is not real. In Process Physics quantum matter are topological defects in the network, but here it is sufficient to give a simple description in terms of an effective density.

We see that there are only four possible terms, and so we need at most three possible constants to parametrise the dynamics of space: G, α and β. G turns out to be Newton's gravitational constant, and describes the rate of non-conservative flow of space into matter. To determine the values of α and β we must, at this stage, turn to experimental data. However most experimental data involving the dynamics of space is observed by detecting the so-called gravitational acceleration

of matter, although increasingly light bending is giving new information. Now the acceleration $\mathbf{a}$ of the dynamical patterns in space is given by the Euler convective expression

$$\mathbf{a}(\mathbf{r},t) = \lim_{\Delta t \to 0} \frac{\mathbf{v}(\mathbf{r}+\mathbf{v}(\mathbf{r},t)\Delta t, t+\Delta t) - \mathbf{v}(\mathbf{r},t)}{\Delta t} = \frac{\partial \mathbf{v}}{\partial t} + (\mathbf{v}.\nabla)\mathbf{v} \qquad (2)$$

and this appears in one of the terms in (1). As shown in [11] and discussed later herein the acceleration $\mathbf{g}$ of quantum matter is identical to this acceleration, apart from vorticity and relativistic effects, and so the gravitational acceleration of matter is also given by (2).

Outside of a spherically symmetric distribution of matter, of total mass M, we find that one solution of (1) is the velocity in-flow field given by

$$\mathbf{v}(\mathbf{r}) = -\hat{\mathbf{r}}\sqrt{\frac{2GM(1+\frac{\alpha}{2}+..)}{r}} \qquad (3)$$

but only when $\beta = -\alpha$, for only then is the acceleration of matter, from (2), induced by this in-flow of the form

$$\mathbf{g}(\mathbf{r}) = -\hat{\mathbf{r}}\frac{GM(1+\frac{\alpha}{2}+..)}{r^2} \qquad (4)$$

which is Newton's Inverse Square Law of 1687 [10], but with an effective mass $M(1+\frac{\alpha}{2}+..)$ that is different from the actual mass M. So the success of Newton's law in the solar system informs us that $\beta = -\alpha$ in (1). But we also see modifications coming from the α-dependent terms.

In general because (1) is a scalar equation it is only applicable for vorticity-free flows $\nabla \times \mathbf{v} = \mathbf{0}$, for then we can write $\mathbf{v} = \nabla u$, and then (1) can always be solved to determine the time evolution of $u(\mathbf{r},t)$ given an initial form at some time t_0. The α-dependent term in (1) (with now $\beta = -\alpha$) and the matter acceleration effect, now also given by (2), permits (1) to be written in the form

$$\nabla.\mathbf{g} = -4\pi G\rho - 4\pi G\rho_{DM}, \qquad (5)$$

where

$$\rho_{DM}(\mathbf{r},t) \equiv \frac{\alpha}{32\pi G}((trD)^2 - tr(D^2)), \qquad (6)$$

which is an effective matter density that would be required to mimic the α-dependent spatial self-interaction dynamics. Then (5) is the differential form for Newton's law of gravity but with an additional non-matter effective matter

density. So we label this as ρ_{DM} even though no matter is involved [37, 38]. This effect has been shown to explain the so-called 'dark matter' effect in spiral galaxies, bore hole g anomalies, and the systematics of galactic black hole masses.

The spatial dynamics is non-local. Historically this was first noticed by Newton who called it action-at-a-distance. To see this we can write (1) as an integro-differential equation

$$\frac{\partial \mathbf{v}}{\partial t} = -\nabla\left(\frac{\mathbf{v}^2}{2}\right) + G\int d^3r' \frac{\rho_{DM}(\mathbf{r}',t)+\rho(\mathbf{r}',t)}{|\mathbf{r}-\mathbf{r}'|^3}(\mathbf{r}-\mathbf{r}') \tag{7}$$

This shows a high degree of non-locality and non-linearity, and in particular that the behaviour of both ρ_{DM} and ρ manifest at a distance irrespective of the dynamics of the intervening space. This non-local behaviour is analogous to that in quantum systems and may offer a resolution to the horizon problem.

However (1) needs to be further generalised [1] to include vorticity, and also the effect of the motion of matter through this substratum via

$$\mathbf{v}_R(\mathbf{r}_0(t),t) = \mathbf{v}_0(t) - \mathbf{v}(\mathbf{r}_0(t),t), \tag{8}$$

where $\mathbf{v}_0(t)$ is the velocity of an object, at $\mathbf{r}_0(t)$, relative to the same frame of reference that defines the flow field; then $\mathbf{v}_R$ is the velocity of that matter relative to the substratum. One possible generalisation of the flow equation (1) is, with $d/dt = \partial/\partial t + \mathbf{v}.\nabla$ the Euler fluid or total derivative,

$$\frac{dD_{ij}}{dt} + \frac{\delta_{ij}}{3}tr(D^2) + \frac{trD}{2}(D_{ij} - \frac{\delta_{ij}}{3}trD) + \frac{\delta_{ij}}{3}\frac{\alpha}{8}((trD)^2 - tr(D^2))$$
$$+(\Omega D - D\Omega)_{ij} = -4\pi G\rho(\frac{\delta_{ij}}{3} + \frac{v_R^i v_R^j}{2c^2} + ..),\ i,j = 1,2,3. \tag{9}$$

$$\nabla\times(\nabla\times\mathbf{v}) = \frac{8\pi G\rho}{c^2}\mathbf{v}_R, \tag{10}$$

$$\Omega_{ij} = \frac{1}{2}(\frac{\partial v_i}{\partial x_j} - \frac{\partial v_j}{\partial x_i}) = -\frac{1}{2}\epsilon_{ijk}\omega_k = -\frac{1}{2}\epsilon_{ijk}(\nabla\times\mathbf{v})_k, \tag{11}$$

and the vorticity vector field is $\vec{\omega} = \nabla\times\mathbf{v}$. For zero vorticity and $v_R \ll c$ (9) reduces to (1). We obtain from (10) the Biot-Savart form for the vorticity

$$\vec{\omega}(\mathbf{r},t) = \frac{2G}{c^2}\int d^3r' \frac{\rho(\mathbf{r}',t)}{|\mathbf{r}-\mathbf{r}'|^3}\mathbf{v}_R(\mathbf{r}',t)\times(\mathbf{r}-\mathbf{r}'). \tag{12}$$

Eqn.(12) has been applied to the precession of gyroscopes in the GP-B satellite experiment, see Sect.10.5.

3 Generalised Schrödinger Equation and Emergent Gravity

Let us consider what might be regarded as the conventional 'Newtonian' approach to including gravity in the Schrödinger equation [11]. There gravity is described by the Newtonian potential energy field $\Phi(\mathbf{r},t)$, such that $\mathbf{g}=-\nabla\Phi$, and we have for a 'free-falling' quantum system, with mass m,

$$i\hbar\frac{\partial\psi(\mathbf{r},t)}{\partial t}=-\frac{\hbar^2}{2m}\nabla^2\psi(\mathbf{r},t)+m\Phi(\mathbf{r},t)\psi(\mathbf{r},t)\equiv H(t)\Psi, \tag{13}$$

where the hamiltonian is in general now time dependent. The classical-limit trajectory is obtained via the usual Ehrenfest method [12]: we first compute the time rate of change of the so-called position 'expectation value'

$$\frac{d<\mathbf{r}>}{dt}\equiv\frac{d}{dt}(\psi,\mathbf{r}\psi)=\frac{i}{\hbar}(H\psi,\mathbf{r}\psi)-\frac{i}{\hbar}(\psi,\mathbf{r}H\psi)=\frac{i}{\hbar}(\psi,[H,\mathbf{r}]\psi), \tag{14}$$

which is valid for a normalised state ψ. The norm is time invariant when H is hermitian ($H^\dagger=H$) even if H itself is time dependent,

$$\frac{d}{dt}(\psi,\psi)=\frac{i}{\hbar}(H\psi,\psi)-\frac{i}{\hbar}(\psi,H\psi)=\frac{i}{\hbar}(\psi,H^\dagger\psi)-\frac{i}{\hbar}(\psi,H\psi)=0. \tag{15}$$

Next we compute the matter 'acceleration' from (14).

$$\begin{aligned}\frac{d^2<\mathbf{r}>}{dt^2} &= \frac{i}{\hbar}\frac{d}{dt}(\psi,[H,\mathbf{r}]\psi),\\ &= \left(\frac{i}{\hbar}\right)^2(\psi,[H,[H,\mathbf{r}]]\psi)+\frac{i}{\hbar}(\psi,[\frac{\partial H(t)}{\partial t},\mathbf{r}]\psi),\\ &= -(\psi,\nabla\Phi\psi)=(\psi,\mathbf{g}(\mathbf{r},t)\psi)=<\mathbf{g}(\mathbf{r},t)>\,.\end{aligned} \tag{16}$$

In the classical limit ψ has the form of a wavepacket where the spatial extent of ψ is much smaller than the spatial region over which $\mathbf{g}(\mathbf{r},t)$ varies appreciably. Then we have the approximation $<\mathbf{g}(\mathbf{r},t)>\approx\mathbf{g}(<\mathbf{r}>,t)$, and finally we arrive at the Newtonian 2nd-law equation of motion for the wavepacket,

$$\frac{d^2<\mathbf{r}>}{dt^2}\approx\mathbf{g}(<\mathbf{r}>,t). \tag{17}$$

In this classical limit we obtain the equivalence principle, namely that the acceleration is independent of the mass m and of the velocity of that mass. But of

course that followed by construction, as the equivalence principle is built into (13) by having m as the coefficient of Φ. In Newtonian gravity there is no explanation for the origin of Φ or $\mathbf{g}$. In the new theory gravity is explained in terms of a velocity field, which in turn has a deeper explanation within *Process Physics*.

The key insight is that conventional physics has neglected the interaction of various systems with the dynamical 3-space. Here we generalise the Schrödinger equation to take account of this new physics. Now gravity is a dynamical effect arising from the time-dependence and spatial inhomogeneities of the 3-space velocity field $\mathbf{v}(\mathbf{r},t)$, and for a 'free-falling' quantum system with mass m the Schrödinger equation now has the generalised form

$$i\hbar\left(\frac{\partial}{\partial t}+\mathbf{v}.\nabla+\frac{1}{2}\nabla.\mathbf{v}\right)\psi(\mathbf{r},t)=-\frac{\hbar^2}{2m}\nabla^2\psi(\mathbf{r},t), \tag{18}$$

which we write as

$$i\hbar\frac{\partial\psi(\mathbf{r},t)}{\partial t}=H(t)\psi(\mathbf{r},t), \quad \text{where} \quad H(t)=-i\hbar\left(\mathbf{v}.\nabla+\frac{1}{2}\nabla.\mathbf{v}\right)-\frac{\hbar^2}{2m}\nabla^2 \tag{19}$$

This form for H specifies how the quantum system must couple to the velocity field, and it uniquely follows from two considerations: (i) the generalised Schrödinger equation must remain form invariant under a change of observer, i.e. with $t\rightarrow t$, and $\mathbf{r}\rightarrow\mathbf{r}+\mathbf{V}t$, where $\mathbf{V}$ is the relative velocity of the two observers. Then we compute that $\frac{\partial}{\partial t}+\mathbf{v}.\nabla+\frac{1}{2}\nabla.\mathbf{v}\rightarrow\frac{\partial}{\partial t}+\mathbf{v}.\nabla+\frac{1}{2}\nabla.\mathbf{v}$, i.e. that it is an invariant operator, and (ii) require that $H(t)$ be hermitian, so that the wavefunction norm is an invariant of the time evolution. This implies that the $\frac{1}{2}\nabla.\mathbf{v}$ term must be included, as $\mathbf{v}.\nabla$ by itself is not hermitian for an inhomogeneous $\mathbf{v}(\mathbf{r},t)$. Then the consequences for the motion of wavepackets are uniquely determined; they are fixed by these two quantum-theoretic requirements.

Then again the classical-limit trajectory is obtained via the position 'expectation value', first with

$$\begin{aligned}\mathbf{v}_O\equiv\frac{d<\mathbf{r}>}{dt} &= \frac{d}{dt}(\psi,\mathbf{r}\psi)=\frac{i}{\hbar}(\psi,[H,\mathbf{r}]\psi)=(\psi,(\mathbf{v}(\mathbf{r},t)-\frac{i\hbar}{m}\nabla)\psi)\\ &= <\mathbf{v}(\mathbf{r},t)>-\frac{i\hbar}{m}<\nabla>,\end{aligned} \tag{20}$$

on evaluating the commutator using $H(t)$ in (19), and which is again valid for a normalised state ψ. Then for the 'acceleration' we obtain from (20) that[1]

$$\frac{d^2<\mathbf{r}>}{dt^2}=\frac{d}{dt}(\psi,(\mathbf{v}-\frac{i\hbar}{m}\nabla)\psi)$$

[1]Care is needed to identify the range of the various ∇'s.

$$
\begin{aligned}
&= (\psi, \left(\frac{\partial \mathbf{v}(\mathbf{r},t)}{\partial t} + \frac{i}{\hbar}[H, (\mathbf{v} - \frac{i\hbar}{m}\nabla)] \right) \psi), \\
&= (\psi, \frac{\partial \mathbf{v}(\mathbf{r},t)}{\partial t}\psi) + (\psi, \left(\mathbf{v}.\nabla + \frac{1}{2}\nabla.\mathbf{v} - \frac{i\hbar}{2m}\nabla^2 \right) \left(\mathbf{v} - \frac{i\hbar}{m}\nabla \right) \psi) - \\
&\quad (\psi, \left(\mathbf{v} - \frac{i\hbar}{m}\nabla \right) \left(\mathbf{v}.\nabla + \frac{1}{2}\nabla.\mathbf{v} - \frac{i\hbar}{2m}\nabla^2 \right) \psi), \\
&= (\psi, \left(\frac{\partial \mathbf{v}(\mathbf{r},t)}{\partial t} + ((\mathbf{v}.\nabla)\mathbf{v}) - \frac{i\hbar}{m}(\nabla \times \mathbf{v}) \times \nabla \right) \psi) + \\
&+ (\psi, \frac{i\hbar}{2m}(\nabla \times (\nabla \times \mathbf{v}))\psi), \\
&\approx \frac{\partial \mathbf{v}}{\partial t} + (\mathbf{v}.\nabla)\mathbf{v} + (\nabla \times \mathbf{v}) \times \left(\frac{d<\mathbf{r}>}{dt} - \mathbf{v} \right) + \frac{i\hbar}{2m}(\nabla \times (\nabla \times \mathbf{v})), \\
&= \frac{\partial \mathbf{v}}{\partial t} + (\mathbf{v}.\nabla)\mathbf{v} + (\nabla \times \mathbf{v}) \times \left(\frac{d<\mathbf{r}>}{dt} - \mathbf{v} \right) \\
&= \frac{\partial \mathbf{v}}{\partial t} + (\mathbf{v}.\nabla)\mathbf{v} + (\nabla \times \mathbf{v}) \times \mathbf{v}_R \qquad (21)
\end{aligned}
$$

where in arriving at the 3rd last line we have invoked the small-wavepacket approximation, and also used (20) to identify

$$\mathbf{v}_R \equiv -\frac{i\hbar}{m} <\nabla> = \mathbf{v}_O - \mathbf{v}, \qquad (22)$$

where $\mathbf{v}_O$ is the velocity of the wavepacket or object 'O' relative to the observer, so then $\mathbf{v}_R$ is the velocity of the wavepacket relative to the local 3-space. Then all velocity field terms are now evaluated at the location of the wavepacket. Note that the operator

$$-\frac{i\hbar}{m}(\nabla \times \mathbf{v}) \times \nabla + \frac{i\hbar}{2m}(\nabla \times (\nabla \times \mathbf{v})) \qquad (23)$$

is hermitian, but that separately neither of these two operators is hermitian. Then in general the scalar product in (21) is real. But then in arriving at the last line in (21) by means of the small-wavepacket approximation, we must then self-consistently use that $\nabla \times (\nabla \times \mathbf{v}) = \mathbf{0}$, otherwise the acceleration acquires a spurious imaginary part. This is consistent with (10) outside of any matter which contributes to the generation of the velocity field, for there $\rho = 0$. These observations point to a deep connection between quantum theory and the velocity field dynamics, as already argued in [1].

We see that the test 'particle' acquires the acceleration of the velocity field, as in (2), and as well an additional vorticity induced acceleration which is the

analogue of the Helmholtz acceleration in fluid mechanics. Then $\vec{\omega}/2$ is the instantaneous angular velocity of the local 3-space, relative to a distant observer. Hence we find that the equivalence principle arises from the unique generalised Schrödinger equation and with the additional vorticity effect. This vorticity effect depends on the absolute velocity $\mathbf{v}_R$ of the object relative to the local space, and so requires a change in the Galilean or Newtonian form of the equivalence principle.

The vorticity acceleration effect is the origin of the Lense-Thirring so-called 'frame-dragging' [2] effect [41] discussed later. While the generation of the vorticity is a relativistic effect, as in (12), the response of the test particle to that vorticity is a non-relativistic effect, and follows from the generalised Schrödinger equation, and which is not present in the standard Schrödinger equation with coupling to the Newtonian gravitational potential, as in (13). Hence the generalised Schrödinger equation with the new coupling to the velocity field is more fundamental. The Helmholtz term in (21) is being explored by the Gravity Probe B gyroscope precession experiment, however the vorticity caused by the motion of the earth is extremely small, as discussed later in Sect.10.5.

An important insight emerges from the above: the generalised Schrödinger equation involves two fields $\mathbf{v}(\mathbf{r},t)$ and $\psi(\mathbf{r},t)$, where the coordinate $\mathbf{r}$ is merely a label to relate the two fields, and is not itself the 3-space. In particular while $\mathbf{r}$ relates to the embedding space, the 3-space itself has time-dependence and inhomogeneities, and as well in the more general case will exhibit vorticity $\vec{\omega} = \nabla \times \mathbf{v}$. Only in the unphysical case does the description of the 3-space become identified with the coordinate system $\mathbf{r}$, and that is when the velocity field $\mathbf{v}(\mathbf{r},t)$ becomes uniform and time independent. Then by a suitable choice of observer we may put $\mathbf{v}(\mathbf{r},t) = \mathbf{0}$, and the generalised Schrödinger equation reduces to the usual 'free' Schrödinger equation. As we discuss later the experimental evidence is that $\mathbf{v}(\mathbf{r},t)$ is fractal and so cannot be removed by a change to a preferred observer. Hence the generalised Schrödinger equation in (19) is a major development for fundamental physics. Of course in general other non-3-space potential energy terms may be added to the RHS of (19). A prediction of this new quantum theory, which also extends to a generalised Dirac equation, is that the fractal structure of space implies that even at the scale of atoms etc there will be time-dependencies and inhomogeneities, and that these will affect transition rates of quantum systems. These effects are probably those known as the Shnoll effects [13].

[2] In the spacetime formalism it is mistakenly argued that it is 'spacetime' that is 'dragged'.

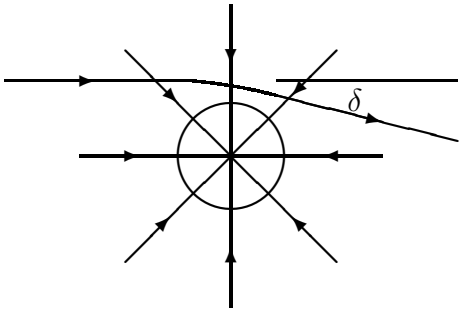

Figure 2: Shows bending of light through angle δ by the inhomogeneous spatial in-flow, according to the minimisation of the travel time in (30). This effect permits the in-flow speed at the surface of the sun to be determined to be 615km/s. The in-flow speed into the sun at the distance of the earth from the sun has been extracted from the Miller data, giving 50 ± 10km/s [1]. Both speeds are in agreement with (3).

4 Generalised Dirac Equation and Relativistic Gravity

An analogous generalisation of the Dirac equation is also necessary giving the coupling of the spinor to the actual dynamical 3-space, and again not to the embedding space as has been the case up until now,

$$i\hbar\frac{\partial\psi}{\partial t} = -i\hbar\left(c\vec{\alpha}.\nabla + \mathbf{v}.\nabla + \frac{1}{2}\nabla.\mathbf{v}\right)\psi + \beta mc^2\psi \tag{24}$$

where $\vec{\alpha}$ and β are the usual Dirac matrices. Repeating the Schrödinger equation analysis for the space-induced acceleration we obtain

$$\mathbf{g} = \frac{\partial\mathbf{v}}{\partial t} + (\mathbf{v}.\nabla)\mathbf{v} + (\nabla\times\mathbf{v})\times\mathbf{v}_R - \frac{\mathbf{v}_R}{1-\frac{\mathbf{v}_R^2}{c^2}}\frac{1}{2}\frac{d}{dt}\left(\frac{\mathbf{v}_R^2}{c^2}\right) \tag{25}$$

which generalises (21) by having a term which limits the speed of the wave packet relative to space to be $< c$. This equation specifies the trajectory of a spinor wave packet in the dynamical 3-space.

5 Generalised Maxwell Equations and Light Lensing

One of the putative key tests of the GR formalism was the gravitational bending of light. This also immediately follows from the new space dynamics once we also generalise the Maxwell equations so that the electric and magnetic fields are

excitations of the dynamical space. The dynamics of the electric and magnetic fields must then have the form, in empty space,

$$\nabla \times \mathbf{E} = -\mu \left(\frac{\partial \mathbf{H}}{\partial t} + \mathbf{v}.\nabla \mathbf{H} \right), \nabla \times \mathbf{H} = \epsilon \left(\frac{\partial \mathbf{E}}{\partial t} + \mathbf{v}.\nabla \mathbf{E} \right), \nabla.\mathbf{H} = \mathbf{0}, \nabla.\mathbf{E} = \mathbf{0} \tag{26}$$

which was first suggested by Hertz in 1890 [14], but with $\mathbf{v}$ being a constant vector field. Suppose we have a uniform flow of space with velocity $\mathbf{v}$ wrt the embedding space or wrt an observer's frame of reference. Then we can find plane wave solutions for (26):

$$\mathbf{E}(\mathbf{r}, t) = \mathbf{E}_0 e^{i(\mathbf{k}.\mathbf{r} - \omega t)} \quad \mathbf{H}(\mathbf{r}, t) = \mathbf{H}_0 e^{i(\mathbf{k}.\mathbf{r} - \omega t)} \tag{27}$$

with

$$\omega(\mathbf{k}, \mathbf{v}) = c|\vec{\mathbf{k}}| + \mathbf{v}.\mathbf{k} \quad \text{where} \quad c = 1/\sqrt{\mu\epsilon} \tag{28}$$

Then the EM group velocity is

$$\mathbf{v}_{EM} = \vec{\nabla}_k \omega(\mathbf{k}, \mathbf{v}) = c\hat{\mathbf{k}} + \mathbf{v} \tag{29}$$

So the velocity of EM radiation $\mathbf{v}_{EM}$ has magnitude c only with respect to the space, and in general not with respect to the observer if the observer is moving through space, as experiment has indicated again and again, as discussed in Sect.9. These experiments show that the speed of light is in general anisotropic, as predicted by (29). The time-dependent and inhomogeneous velocity field causes the refraction of EM radiation. This can be computed by using the Fermat least-time approximation. Then the EM ray paths $\mathbf{r}(t)$ are determined by minimising the elapsed travel time:

$$\tau = \int_{s_i}^{s_f} \frac{ds|\frac{d\mathbf{r}}{ds}|}{|c\hat{\mathbf{v}}_R(s) + \mathbf{v}(\mathbf{r}(\mathbf{s}), \mathbf{t}(\mathbf{s})|} \quad \text{with} \quad \mathbf{v}_R = \left(\frac{d\mathbf{r}}{dt} - \mathbf{v}(\mathbf{r}(\mathbf{t}), \mathbf{t}) \right) \tag{30}$$

by varying both $\mathbf{r}(s)$ and $t(s)$, finally giving $\mathbf{r}(t)$. Here s is a path parameter, and $\mathbf{v}_R$ is a 3-space tangent vector for the path. As an example, the in-flow in (3), which is applicable to light bending by the sun, gives the angle of deflection

$$\delta = 2\frac{v^2}{c^2} = \frac{4GM(1 + \frac{\alpha}{2} + ..)}{c^2 d} + ... \tag{31}$$

where v is the in-flow speed at distance d and d is the impact parameter. This agrees with the GR result except for the α correction. Hence the observed deflection of 8.4×10^{-6} radians is actually a measure of the in-flow speed at the

sun's surface, and that gives $v = 615$km/s. These generalised Maxwell equations also predict gravitational lensing produced by the large in-flows associated with the new 'black holes' in galaxies, see [15]. So again this effect permits the direct observation of the these black hole effects with their non inverse-square-law accelerations.

6 Free-Fall Minimum Proper-Time Trajectories

The acceleration in (25) also arises from the following argument, which is the analogue of the Fermat least-time formalism for the quantum matter waves. Consider the elapsed time for a comoving clock. Then taking account of the Lamour time-dilation effect that time is given by

$$\tau[\mathbf{r}_0] = \int dt \left(1 - \frac{\mathbf{v}_R^2}{c^2}\right)^{1/2} \tag{32}$$

with $\mathbf{v}_R$ given by (22) in terms of $\mathbf{v}_O$ and $\mathbf{v}$. Then this time effect relates to the speed of the clock relative to the local 3-space, and that c is the speed of light relative to that local 3-space. Under a deformation of the trajectory

$$\mathbf{r}_0(t) \to \mathbf{r}_0(t) + \delta\mathbf{r}_0(t), \quad \mathbf{v}_0(t) \to \mathbf{v}_0(t) + \frac{d\delta\mathbf{r}_0(t)}{dt}, \tag{33}$$

$$\mathbf{v}(\mathbf{r}_0(t) + \delta\mathbf{r}_0(t), t) = \mathbf{v}(\mathbf{r}_0(t), t) + (\delta\mathbf{r}_0(t).\nabla)\mathbf{v}(\mathbf{r}_0(t), t) + ... \tag{34}$$

Evaluating the change in proper travel time to lowest order

$$\begin{aligned}
\delta\tau &= \tau[\mathbf{r}_0 + \delta\mathbf{r}_0] - \tau[\mathbf{r}_0] + ... \\
&= -\int dt\, \frac{1}{c^2}\mathbf{v}_R.\delta\mathbf{v}_R \left(1 - \frac{\mathbf{v}_R^2}{c^2}\right)^{-1/2} + ... \\
&= \int dt \frac{1}{c^2} \frac{\mathbf{v}_R.(\delta\mathbf{r}_0.\nabla)\mathbf{v} - \mathbf{v}_R.\dfrac{d(\delta\mathbf{r}_0)}{dt}}{\sqrt{1 - \dfrac{\mathbf{v}_R^2}{c^2}}} + ... \\
&= \int dt \frac{1}{c^2} \left(\frac{\mathbf{v}_R.(\delta\mathbf{r}_0.\nabla)\mathbf{v}}{\sqrt{1 - \dfrac{\mathbf{v}_R^2}{c^2}}} + \delta\mathbf{r}_0.\frac{d}{dt}\frac{\mathbf{v}_R}{\sqrt{1 - \dfrac{\mathbf{v}_R^2}{c^2}}} \right) + ...
\end{aligned}$$

$$= \int dt\, \frac{1}{c^2}\delta\mathbf{r}_0 \,.\, \left(\frac{(\mathbf{v}_R.\nabla)\mathbf{v} + \mathbf{v}_R \times (\nabla \times \mathbf{v})}{\sqrt{1 - \frac{\mathbf{v}_R^2}{c^2}}} + \frac{d}{dt}\frac{\mathbf{v}_R}{\sqrt{1 - \frac{\mathbf{v}_R^2}{c^2}}} \right) + ...$$

Hence a trajectory $\mathbf{r}_0(t)$ determined by $\delta\tau = 0$ to $O(\delta\mathbf{r}_0(t)^2)$ satisfies

$$\frac{d}{dt}\frac{\mathbf{v}_R}{\sqrt{1 - \frac{\mathbf{v}_R^2}{c^2}}} = -\frac{(\mathbf{v}_R.\nabla)\mathbf{v} + \mathbf{v}_R \times (\nabla \times \mathbf{v})}{\sqrt{1 - \frac{\mathbf{v}_R^2}{c^2}}}. \tag{35}$$

Substituting $\mathbf{v}_R(t) = \mathbf{v}_0(t) - \mathbf{v}(\mathbf{r}_0(t), t)$ and using

$$\frac{d\mathbf{v}(\mathbf{r}_0(t), t)}{dt} = \frac{\partial \mathbf{v}}{\partial t} + (\mathbf{v}_0.\nabla)\mathbf{v}, \tag{36}$$

we obtain

$$\frac{d\mathbf{v}_0}{dt} = \frac{\partial \mathbf{v}}{\partial t} + (\mathbf{v}.\nabla)\mathbf{v} + (\nabla \times \mathbf{v}) \times \mathbf{v}_R - \frac{\mathbf{v}_R}{1 - \frac{\mathbf{v}_R^2}{c^2}} \frac{1}{2}\frac{d}{dt}\left(\frac{\mathbf{v}_R^2}{c^2}\right). \tag{37}$$

which is (25). Then in the low speed limit $v_R \ll c$ we may neglect the last term, and we obtain (21). Hence we see a close relationship between the geodesic equation, known first from General Relativity, and the 3-space generalisation of the Schrödinger equation, at least in the non-relativistic limit. So in the classical limit, i.e when the wavepacket approximation is valid, the wavepacket trajectory is specified by the least proper-time geodesic.

The relativistic term in (37) is responsible for the precession of elliptical orbits and also for the event horizon effect. Hence the trajectory in (21) is a non-relativistic minimum travel-time trajectory, which is Fermat's Principle.

7 Deriving the Special Relativity Formalism

The detection of absolute motion is not incompatible with Lorentz symmetry; the contrary belief was postulated by Einstein, and has persisted for over 100 years, since 1905. So far the experimental evidence is that absolute motion and Lorentz symmetry are real and valid phenomena; absolute motion is motion relative to some substructure to space, whereas Lorentz symmetry parametrises

dynamical effects caused by the motion of systems through that substructure. Motion through the structured space, it is argued, induces actual dynamical time dilations and length contractions in agreement with the Lorentz interpretation of special relativistic effects. Then observers in uniform motion 'through' the space will, on measurement of the speed of light using the special but misleading Einstein measurement protocol, obtain always the same numerical value c. To see this explicitly consider how various observers $P, P', \ldots$ moving with different speeds through space, measure the speed of light. They each acquire a standard rod and an accompanying standardised clock. That means that these standard rods would agree if they were brought together, and at rest with respect to space they would all have length Δl_0, and similarly for the clocks. Observer P and accompanying rod are both moving at speed v_R relative to space, with the rod longitudinal to that motion. P then measures the time Δt_R, with the clock at end A of the rod, for a light pulse to travel from end A to the other end B and back again to A. The light travels at speed c relative to space. Let the time taken for the light pulse to travel from $A \to B$ be t_{AB} and from $B \to A$ be t_{BA}, as measured by a clock at rest with respect to space[3]. The length of the rod moving at speed v_R is contracted to

$$\Delta l_R = \Delta l_0 \sqrt{1 - \frac{v_R^2}{c^2}}\,. \tag{38}$$

In moving from A to B the light must travel an extra distance because the end B travels a distance $v_R t_{AB}$ in this time, thus the total distance that must be traversed is

$$c t_{AB} = \Delta l_R + v_R\, t_{AB}\,, \tag{39}$$

similarly on returning from B to A the light must travel the distance

$$c t_{BA} = \Delta l_R - v_R\, t_{BA}\,. \tag{40}$$

Hence the total travel time Δt_0 is

$$\Delta t_0 = t_{AB} + t_{BA} = \frac{\Delta l_R}{c - v_R} + \frac{\Delta l_R}{c + v_R} == \frac{2\Delta l_0}{c\sqrt{1 - \frac{v_R^2}{c^2}}}\,. \tag{41}$$

Because of the time dilation effect for the moving clock

$$\Delta t_R = \Delta t_0 \sqrt{1 - \frac{v_R^2}{c^2}}\,. \tag{42}$$

[3]Not all clocks will behave in this same "ideal" manner.

Then for the moving observer the speed of light is defined as the distance the observer believes the light travelled ($2\Delta l_0$) divided by the travel time according to the accompanying clock (Δt_R), namely $2\Delta l_0/\Delta t_R = c$, from above, which is thus the same speed as seen by an observer at rest in the space, namely c. So the speed v_R of the observer through space is not revealed by this procedure, and the observer is erroneously led to the conclusion that the speed of light is always c. This follows from two or more observers in manifest relative motion all obtaining the same speed c by this procedure. Despite this failure this special effect is actually the basis of the spacetime Einstein measurement protocol. That this protocol is blind to the absolute motion has led to enormous confusion within physics.

To be explicit the Einstein measurement protocol actually inadvertently uses this special effect by using the radar method for assigning historical spacetime coordinates to an event: the observer records the time of emission and reception of radar pulses ($t_r > t_e$) travelling through space, and then retrospectively assigns the time and distance of a distant event B according to (ignoring directional information for simplicity)

$$T_B = \frac{1}{2}\,(t_r + t_e)\,, \qquad D_B = \frac{c}{2}\,(t_r - t_e)\,, \tag{43}$$

where each observer is now using the same numerical value of c. The event B is then plotted as a point in an individual geometrical construct by each observer, known as a spacetime record, with coordinates (D_B, T_B). This is the same as an historian recording events according to some agreed protocol. Unlike historians, who don't confuse history books with reality, physicists do so. We now show that because of this protocol and the absolute motion dynamical effects, observers will discover on comparing their historical records of the same events that the expression

$$\tau_{AB}^2 = T_{AB}^2 - \frac{1}{c^2}\,D_{AB}^2\,, \tag{44}$$

is an invariant, where $T_{AB} = T_A - T_B$ and $D_{AB} = D_A - D_B$ are the differences in times and distances assigned to events A and B using the Einstein measurement protocol (43), so long as both are sufficiently small compared with the scale of inhomogeneities in the velocity field.

To confirm the invariant nature of the construct in (44) one must pay careful attention to observational times as distinct from protocol times and distances, and this must be done separately for each observer. This can be tedious. We now demonstrate this for the situation illustrated in Fig. 3.

By definition the speed of P' according to P is $v_0' = D_B/T_B$ and so $v_R' = v_0'$, where T_B and D_B are the protocol time and distance for event B for observer P

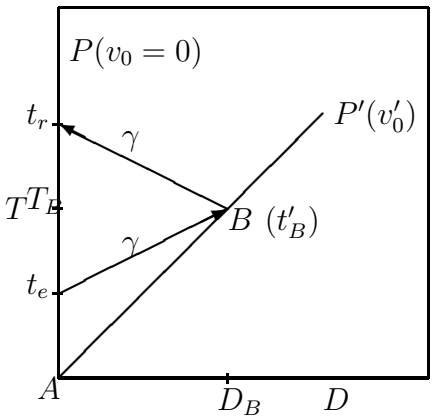

Figure 3: Here $T-D$ is the spacetime construct (from the Einstein measurement protocol) of a special observer P *at rest* wrt space, so that $v_0 = 0$. Observer P' is moving with speed v_0' as determined by observer P, and therefore with speed $v_R' = v_0'$ wrt space. Two light pulses are shown, each travelling at speed c wrt both P and space. Event A is when the observers pass, and is also used to define zero time for each for convenience.

according to (43). Then using (44) P would find that $(\tau_{AB}^P)^2 = T_B^2 - \frac{1}{c^2}D_B^2$ since both $T_A = 0$ and D_A=0, and whence $(\tau_{AB}^P)^2 = (1 - \frac{v_R'^2}{c^2})T_B^2 = (t_B')^2$ where the last equality follows from the time dilation effect on the P' clock, since t_B' is the time of event B according to that clock. Then T_B is also the time that P' would compute for event B when correcting for the time-dilation effect, as the speed v_R' of P' through the quantum foam is observable by P'. Then T_B is the 'common time' for event B assigned by both observers. For P' we obtain directly, also from (43) and (44), that $(\tau_{AB}^{P'})^2 = (T_B')^2 - \frac{1}{c^2}(D_B')^2 = (t_B')^2$, as $D_B' = 0$ and $T_B' = t_B'$. Whence for this situation

$$(\tau_{AB}^P)^2 = (\tau_{AB}^{P'})^2, \tag{45}$$

and so the construction (44) is an invariant.

While so far we have only established the invariance of the construct (44) when one of the observers is at rest in space, it follows that for two observers P' and P'' both in absolute motion it follows that they also agree on the invariance of (44). This is easily seen by using the intermediate step of a stationary observer P:

$$(\tau_{AB}^{P'})^2 = (\tau_{AB}^P)^2 = (\tau_{AB}^{P''})^2. \tag{46}$$

Hence the protocol and Lorentzian absolute motion effects result in the construction in (44) being indeed an invariant in general. This is a remarkable and subtle result. For Einstein this invariance was a fundamental assumption, but here it is a derived result, but one which is nevertheless deeply misleading. Explicitly indicating small quantities by Δ prefixes, and on comparing records retrospectively, an ensemble of nearby observers agree on the invariant

$$\Delta\tau^2 = \Delta T^2 - \frac{1}{c^2}\,\Delta D^2, \tag{47}$$

for any two nearby events. This implies that their individual patches of spacetime records may be mapped one into the other merely by a change of coordinates, and that collectively the spacetime patches of all may be represented by one pseudo-Riemannian manifold, where the choice of coordinates for this manifold is arbitrary, and we finally arrive at the invariant

$$\Delta\tau^2 = g_{\mu\nu}(x)\,\Delta x^\mu \Delta x^\nu, \tag{48}$$

with $x^\mu = \{D_1, D_2, D_3, T\}$. Eqn. (48) is invariant under the Lorentz transformations

$$x'^\mu = L^\mu{}_\nu\, x^\nu, \tag{49}$$

where, for example for relative motion in the x direction, $L^\mu{}_\nu$ is specified by

$$x' = \frac{x - vt}{\sqrt{1 - v^2/c^2}}\,, \quad y' = y, \quad z' = z, \quad t' = \frac{t - vx/c^2}{\sqrt{1 - v^2/c^2}} \tag{50}$$

So absolute motion and special relativity effects, and even Lorentz symmetry, are all compatible: a possible preferred frame is hidden by the Einstein measurement protocol.

The experimental question is then whether or not a supposed preferred frame actually exists or not — can it be detected experimentally? The answer is that there are now eight such consistent experiments.

The notion that the special relativity formalism requires that the speed of light be isotropic, that it be c in all frames, has persisted for most of the last century. The actual situation is that it only requires that the round trip speed be invariant. This means that the famous Einstein light speed postulate is actually incorrect. This is discussed in [27, 28, 29, 30, 31].

8 Deriving the General Relativity Formalism

As discussed above the generalised Dirac equation gives rise to a trajectory determined by (25), which may be obtained by extremising the time-dilated elapsed time (32).

$$\tau[\mathbf{r}_0] = \int dt \left(1 - \frac{\mathbf{v}_R^2}{c^2}\right)^{1/2} \tag{51}$$

This happens because of the Fermat least-time effect for quantum matter waves: only along the minimal time trajectory do the quantum waves remain in phase

under small variations of the path. This again emphasises that gravity is a quantum effect. We now introduce a spacetime mathematical construct according to the metric

$$ds^2 = dt^2 - (d\mathbf{r} - \mathbf{v}(\mathbf{r},t)dt)^2/c^2 = g_{\mu\nu}dx^\mu dx^\nu \tag{52}$$

Then according to this metric the elapsed time in (51) is

$$\tau = \int dt \sqrt{g_{\mu\nu}\frac{dx^\mu}{dt}\frac{dx^\nu}{dt}}, \tag{53}$$

and the minimisation of (53) leads to the geodesics of the spacetime, which are thus equivalent to the trajectories from (51), namely (25). Hence by coupling the Dirac spinor dynamics to the 3-space dynamics we derive the geodesic formalism of General Relativity as a quantum effect, but without reference to the Hilbert-Einstein equations for the induced metric. Indeed in general the metric of this induced spacetime will not satisfy these equations as the dynamical space involves the α-dependent dynamics, and α is missing from GR. So why did GR appear to succeed in a number of key tests where the Schwarzschild metric was used? The answer is provided by identifying the induced spacetime metric corresponding to the in-flow in (3) outside of a spherical matter system, such as the earth. Then (52) becomes

$$ds^2 = dt^2 - \frac{1}{c^2}(dr + \sqrt{\frac{2GM(1+\frac{\alpha}{2}+..)}{r}}dt)^2 - \frac{1}{c^2}r^2(d\theta^2 + \sin^2(\theta)d\phi^2), \tag{54}$$

Making the change of variables $t \to t'$ and $\mathbf{r} \to \mathbf{r}' = \mathbf{r}$ with

$$t' = t - \frac{2}{c}\sqrt{\frac{2GM(1+\frac{\alpha}{2}+\ldots)r}{c^2}} + \frac{4\ GM(1+\frac{\alpha}{2}+\ldots)}{c^3}\tanh^{-1}\sqrt{\frac{2GM(1+\frac{\alpha}{2}+\ldots)}{c^2 r}} \tag{55}$$

this becomes (and now dropping the prime notation)

$$\begin{aligned} ds^2 &= \left(1 - \frac{2GM(1+\frac{\alpha}{2}+..)}{c^2 r}\right)dt^2 - \frac{1}{c^2}r^2(d\theta^2 + \sin^2(\theta)d\phi^2) \\ &\quad - \frac{dr^2}{c^2\left(1 - \frac{2GM(1+\frac{\alpha}{2}+..)}{c^2 r}\right)}. \end{aligned} \tag{56}$$

which is one form of the the Schwarzschild metric but with the α-dynamics induced effective mass shift. Of course this is only valid outside of the spherical

matter distribution, as that is the proviso also on (3). As well the above particular change of coordinates also introduces spurious singularities at the event horizon[4], but other choices do not do this. Hence in the case of the Schwarzschild metric the dynamics missing from both the Newtonian theory of gravity and General Relativity is merely hidden in a mass redefinition, and so didn't affect the various standard tests of GR, or even of Newtonian gravity. Note that as well we see that the Schwarzschild metric is none other than Newtonian gravity in disguise, except for the mass shift. While we have now explained why the GR formalism appeared to work, it is also clear that this formalism hides the manifest dynamics of the dynamical space, and which has also been directly detected in gas-mode interferometer and coaxial-cable experiments.

Nevertheless we now show [1] that in the limit $\alpha \to 0$ the induced metric in (52), with $\mathbf{v}$ from (1), satisfies the Hilbert-Einstein equations so long as we use relativistic corrections for the matter density on the RHS of (1). This means that (1) is consistent with for example the binary pulsar data - the relativistic aspects being associated with the matter effects upon space and the relativistic effects of the matter in motion through the dynamical 3-space. The agreement of GR with the pulsar data is implying that the α-dependent effects are small in this case, unlike in black holes and spiral galaxies. The GR equations are

$$G_{\mu\nu} \equiv R_{\mu\nu} - \frac{1}{2}Rg_{\mu\nu} = \frac{8\pi G}{c^2}T_{\mu\nu}, \tag{57}$$

where $G_{\mu\nu}$ is the Einstein tensor, $T_{\mu\nu}$ is the energy-momentum tensor, $R_{\mu\nu} = R^{\alpha}_{\mu\alpha\nu}$ and $R = g^{\mu\nu}R_{\mu\nu}$ and $g^{\mu\nu}$ is the matrix inverse of $g_{\mu\nu}$. The curvature tensor is

$$R^{\rho}_{\mu\sigma\nu} = \Gamma^{\rho}_{\mu\nu,\sigma} - \Gamma^{\rho}_{\mu\sigma,\nu} + \Gamma^{\rho}_{\alpha\sigma}\Gamma^{\alpha}_{\mu\nu} - \Gamma^{\rho}_{\alpha\nu}\Gamma^{\alpha}_{\mu\sigma}, \tag{58}$$

where $\Gamma^{\alpha}_{\mu\sigma}$ is the affine connection

$$\Gamma^{\alpha}_{\mu\sigma} = \frac{1}{2}g^{\alpha\nu}\left(\frac{\partial g_{\nu\mu}}{\partial x^{\sigma}} + \frac{\partial g_{\nu\sigma}}{\partial x^{\mu}} - \frac{\partial g_{\mu\sigma}}{\partial x^{\nu}}\right). \tag{59}$$

Let us substitute the metric in (52) into (57) using (58) and (59). The various components of the Einstein tensor are then found to be

$$\begin{aligned} G_{00} &= \sum_{i,j=1,2,3} v_i\mathcal{G}_{ij}v_j - c^2\sum_{j=1,2,3}\mathcal{G}_{0j}v_j - c^2\sum_{i=1,2,3} v_i\mathcal{G}_{i0} + c^2\mathcal{G}_{00}, \\ G_{i0} &= -\sum_{j=1,2,3}\mathcal{G}_{ij}v_j + c^2\mathcal{G}_{i0}, \qquad G_{ij} = \mathcal{G}_{ij}, \qquad i,j = 1,2,3. \end{aligned} \tag{60}$$

[4]The event horizon of (56) is at a different radius from the actual event horizon of the black hole solutions that arise from (1).

where the $\mathcal{G}_{\mu\nu}$ are given by

$$\begin{aligned}\mathcal{G}_{00} &= \frac{1}{2}((trD)^2 - tr(D^2)), \quad \mathcal{G}_{i0} = \mathcal{G}_{0i} = -\frac{1}{2}(\nabla \times (\nabla \times \mathbf{v}))_i, \quad i = 1, 2, 3. \\ \mathcal{G}_{ij} &= \frac{d}{dt}(D_{ij} - \delta_{ij} trD) + (D_{ij} - \frac{1}{2}\delta_{ij} trD)trD - \frac{1}{2}\delta_{ij} tr(D^2) + (\Omega D - D\Omega)_{ij}, \\ & \qquad i, j = 1, 2, 3. \end{aligned} \tag{61}$$

In vacuum, with $T_{\mu\nu} = 0$, we find from (57) and (60) that $G_{\mu\nu} = 0$ implies that $\mathcal{G}_{\mu\nu} = 0$. We see that the Hilbert-Einstein equations demand that

$$(trD)^2 - tr(D^2) = 0 \tag{62}$$

but it is these terms in (1) that explain the various gravitational anomalies. This simply corresponds to the fact that GR does not permit the 'dark matter' effect, and this happens because GR was forced to agree with Newtonian gravity, in the appropriate limits, and that theory also has no such effect. As well in GR the energy-momentum tensor $T_{\mu\nu}$ is not permitted to make any reference to absolute linear motion of the matter; only the relative motion of matter or absolute rotational motion is permitted, contrary to the experiments.

It is very significant to note that the above exposition of the GR formalism for the metric in (52) is exact. Then taking the trace of the $\mathcal{G}_{ij}$ equation in (61) we obtain, also exactly, and in the case of zero vorticity, and outside of matter so that $T_{\mu\nu} = 0$,

$$\frac{\partial}{\partial t}(\nabla.\mathbf{v}) + \nabla.((\mathbf{v}.\nabla)\mathbf{v}) = 0 \tag{63}$$

which is the Newtonian 'velocity field' formulation of Newtonian gravity outside of matter, as in (1) but with $\alpha = \beta = 0$. So GR turns out to be Newtonian gravity in a grossly overstructured mathematical formalism.

9 Experimental and Observational Phenomena I

We now briefly review the extensive range of light speed experiments that have detected that the speed of light is not isotropic - the speed is different in different directions when measured in a laboratory experiment on earth, as predicted by the generalised Maxwell equations, Sect.5. The most famous of these experiments was that of Michelson and Morley in 1887. Contrary to often repeated

claims, this experiment decisively detected the anisotropy. The cause of the misunderstanding surrounding this experiment is that the Newtonian based theory Michelson used for the calibration of the experiment is simply wrong, and of course not unexpectedly. Clearly as the Michelson interferometer is a 2nd order v/c experiment its calibration requires a 'relativistic' analysis, in particular one must take account of arm contractions and also the Fresnel drag effect. The Michelson-Morley fringe shift data then gives a speed in excess of 300km/s, as first discovered by Cahill and Kitto in 2002 [17].

9.1 Anisotropy of the Speed of Light

That the speed of light in vacuum is the same in all directions, i.e. isotropic, for all observers has been taken as a critical assumption in the standard formulation of fundamental physics, and was introduced by Einstein in 1905 as one of his key postulates when formulating his interpretation of Special Relativity. The need to detect any anisotropy has challenged physicists from the 19th century to the present day, particularly following the Michelson-Morley experiment of 1887. The problem arose when Maxwell in 1861 successfully computed the speed of light c from his unified theory of electric and magnetic fields: but what was the speed c relative to? There have been many attempts to detect any supposed light-speed anisotropy and there have so far been 8 successful and consistent such experiments, and as well numerous unsuccessful experiments, i.e. experiments in which no anisotropy was observed. The reasons for these different outcomes is now understood: any light-speed anisotropy produces not only an expected 'direct' effect, being that which is expected to produce a 'signal', but also affects the very physical structure of the apparatus, and with this effect usually overlooked in the design of some detectors. In some designs these effects exactly cancel. As already stated there is overwhelming evidence from 8 experiments that the speed of light is anisotropic, and with a *large* anisotropy at the level of 1 part in 10^3: so these experiments show that a dynamical 3-space exists, and that the spacetime concept was only a mathematical construct - it does not exist as an entity of reality, it has no ontological significance. These developments have lead to a new physics in which the dynamics of the 3-space have been formulated, together with the required generalisations of the Maxwell equations (as first suggested by Hertz in 1890 [14]), and of the Schrödinger and Dirac equations, which have lead to the new emergent theory and explanation of gravity, with numerous confirmations of that theory from the data from black hole systematics, light bending, spiral galaxy rotation anomalies, bore hole anomalies, etc. This data has revealed that

the coupling constant for the self-interaction of the dynamical 3-space is none other than the fine structure constant $\approx 1/137$ [37, 38, 39, 40], which suggests an emerging unified theory of quantum matter and a quantum foam description of the dynamical 3-space.

The most influential of the early attempts to detect any anisotropy in the speed of light was the Michelson-Morley experiment of 1887, [2]. Despite that, and its influence on physics, its operation was only finally understood in 2002 [16, 17, 18]. The problem has been that the Michelson interferometer has a major flaw in its design, when used to detect any light-speed anisotropy effect[5]. To see this requires use of Special Relativity effects. The Michelson interferometer compares the round-trip light travel time in two orthogonal arms, by means of interference fringe shifts measuring time differences, as the device is rotated. However if the device is operated in vacuum, any anticipated change in the total travel times caused by the light travelling at different speeds in the outward and inward directions is exactly cancelled by the Fitzgerald-Lorentz mirror-supporting-arm contraction effect - a real physical effect. Of course this is precisely how Fitzgerald and Lorentz independently arrived at the idea of the length contraction effect. In vacuum this means that the round-trip travel times in each arm *do not* change during rotation. This is the fatal design flaw that has confounded physics for over 100 years. However the cancellation of a supposed change in the round-trip travel times and the Lorentz contraction effect is merely an incidental flaw of the Michelson interferometer. The critical observation is that if we have a gas in the light path, the round-trip travel times are changed, but the Lorentz arm-length contraction effect is unchanged, and then these effects no longer exactly cancel. Not surprisingly the fringe shifts are now proportional to $n - 1$, where n is the refractive index of the gas. Of course with a gas present one must also take account of the Fresnel drag effect, because the gas itself is in absolute motion. This is an important effect, so large in fact that it reverses the sign of the time differences between the two arms, although in operation that is not a problem. As well, since for example for air $n = 1.00029$ at STP, the sensitivity of the interferometer is very low. Nevertheless the Michelson-Morley experiment as well as the Miller interferometer experiment of 1925/1926 [3] were done in air, which is why they indeed observed and reported fringe shifts. As well Illingworth [19] and Joos [20] used helium gas in the light paths in their Michelson interferometers; taking account of that brings their results into agreement with those of the air interferometer experiment, and so confirming the refractive index effect. Jaseja *et*

[5]Which also severely diminishes its use in long-baseline interferometers built to detect gravitational waves.

al. [21] used a He-Ne gas mixture of unknown refractive index, but again detected fringe shifts on rotation. A re-analysis of the data from the above experiments, particularly from the enormous data set of Miller, has revealed that a large light-speed anisotropy had been detected from the very beginning of such experiments, where the speed is some 430 ± 20km/s - this is in excess of 1 part in 10^3, and the Right Ascension and Declination of the direction was determined by Miller [3] long ago. We also briefly review the RF coaxial cable speed experiments of Torr and Kolen [22], DeWitte [23] and Cahill [24], which agree with the gas-mode Michelson interferometer experiments.

9.2 Michelson Gas-mode Interferometer

Let us first consider the new understanding of how the Michelson interferometer works. This brilliant but very subtle device was conceived by Michelson as a means to detect the anisotropy of the speed of light, as was expected towards the end of the 19th century. Michelson used Newtonian physics to develop the theory and hence the calibration for his device. However we now understand that this device detects 2nd order effects in v/c to determine v, and so we must take account of relativistic effects. However the application and analysis of data from various Michelson interferometer experiments using a relativistic theory only occurred in 2002, some 97 years after the development of Special Relativity by Einstein, and some 115 years after the famous 1887 experiment. As a consequence of the necessity of using relativistic effects it was discovered in 2002 that the gas in the light paths plays a critical role, and that we finally understand how to calibrate the device, and we also discovered, some 76 years after the 1925/26 Miller experiment, what determines the calibration constant k that Miller had determined using the Earth's rotation speed about the Sun to set the calibration. This, as we discuss later, has enabled us to now appreciate that gas-mode Michelson interferometer experiments have confirmed the reality of the Fitzgerald-Lorentz length contraction effect: in the usual interpretation of Special Relativity this effect, and others, is usually regarded as an observer dependent effect, an illusion induced by the spacetime. But the experiments are to the contrary showing that the length contraction effect is an actual observer-independent dynamical effect, as Fitzgerald and Lorentz had proposed.

The Michelson interferometer compares the change in the difference between travel times, when the device is rotated, for two coherent beams of light that travel in orthogonal directions between mirrors; the changing time difference being indicated by the shift of the interference fringes during the rotation. This

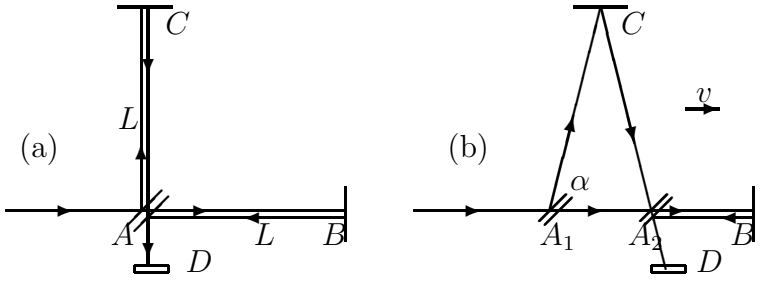

Figure 4: Schematic diagrams of the Michelson Interferometer, with beamsplitter/mirror at A and mirrors at B and C on arms from A, with the arms of equal length L when at rest. D is a screen or detector. In (a) the interferometer is at rest in space. In (b) the interferometer is moving with speed v relative to space in the direction indicated. Interference fringes are observed at the detector D. If the interferometer is rotated in the plane through 90^o, the roles of arms AC and AB are interchanged, and during the rotation shifts of the fringes are seen in the case of absolute motion, but only if the apparatus operates in a gas. By counting fringe changes the speed v may be determined.

effect is caused by the absolute motion of the device through 3-space with speed v, and that the speed of light is relative to that 3-space, and not relative to the apparatus/observer. However to detect the speed of the apparatus through that 3-space gas must be present in the light paths for purely technical reasons. The post relativistic-effects theory for this device is remarkably simple. Consider here only the case where the arms are parallel/anti-parallel to the direction of absolute motion. The relativistic Fitzgerald-Lorentz contraction effect causes the arm AB parallel to the absolute velocity to be physically contracted to length (see Fig.4)

$$L_{||} = L\sqrt{1 - \frac{v^2}{c^2}}\,. \tag{64}$$

The time t_{AB} to travel AB is set by $Vt_{AB} = L_{||} + vt_{AB}$, while for BA by $Vt_{BA} = L_{||} - vt_{BA}$, where $V = c/n$ is the speed of light, with n the refractive index of the gas present. For simplicity we ignore here the Fresnel drag effect, an effect caused by the gas also being in absolute motion, see [1]. The Fresnel drag effect is actually large, and results in a change of sign in (67) and (68). For the total ABA travel time we then obtain

$$t_{ABA} = t_{AB} + t_{BA} = \frac{2LV}{V^2 - v^2}\sqrt{1 - \frac{v^2}{c^2}}\,. \tag{65}$$

For travel in the AC direction we have, from the Pythagoras theorem for the right-angled triangle in Fig.4 that $(Vt_{AC})^2 = L^2 + (vt_{AC})^2$ and that $t_{CA} = t_{AC}$.

Then for the total ACA travel time

$$t_{ACA} = t_{AC} + t_{CA} = \frac{2L}{\sqrt{V^2 - v^2}}\,. \tag{66}$$

Then the difference in travel time is

$$\Delta t = \frac{(n^2-1)\,L}{c}\frac{v^2}{c^2} + \mathrm{O}\left(\frac{v^4}{c^4}\right). \tag{67}$$

after expanding in powers of v/c. This clearly shows that the interferometer can only operate as a detector of absolute motion when not in vacuum ($n = 1$), namely when the light passes through a gas, as in the early experiments (in transparent solids a more complex phenomenon occurs). A more general analysis [1] with the arms at angle θ to $\mathbf{v}$ gives

$$\Delta t = k^2\frac{Lv_P^2}{c^3}\cos(2(\theta-\psi)), \tag{68}$$

where ψ specifies the direction of $\mathbf{v}$ projected onto the plane of the interferometer relative to the local meridian, and where $k^2 \approx n(n^2-1)$. Neglect of the relativistic Fitzgerald-Lorentz contraction effect gives $k^2 \approx n^3 \approx 1$ for gases, which is essentially the Newtonian theory that Michelson used.

However the above analysis does not correspond to how the interferometer is actually operated. That analysis does not actually predict fringe shifts for the field of view would be uniformly illuminated, and the observed effect would be a changing level of luminosity rather than fringe shifts. As Miller knew, the mirrors must be made slightly non-orthogonal with the degree of non-orthogonality determining how many fringe shifts were visible in the field of view. Miller experimented with this effect to determine a comfortable number of fringes: not too few and not too many. Hicks [25] developed a theory for this effect — however it is not necessary to be aware of this analysis in using the interferometer: the non-orthogonality reduces the symmetry of the device, and instead of having period of 180° the symmetry now has a period of 360°, so that to (68) we must add the extra term $a\cos(\theta-\beta)$ in

$$\Delta t = k^2\frac{L(1+e\theta)v_P^2}{c^3}\cos(2(\theta-\psi)) + a(1+e\theta)\cos(\theta-\beta) + f \tag{69}$$

The term $1 + e\theta$ models the temperature effects, namely that as the arms are uniformly rotated, one rotation taking several minutes, there will be a temperature induced change in the length of the arms. If the temperature effects are

linear in time, as they would be for short time intervals, then they are linear in θ. In the Hick's term the parameter a is proportional to the length of the arms, and so also has the temperature factor. The term f simply models any offset effect. Michelson and Morley and Miller took these two effects into account when analysing his data. The Hick's effect is particularly apparent in the Miller and Michelson-Morley data.

The interferometers are operated with the arms horizontal. Then in (69) θ is the azimuth of one arm relative to the local meridian, while ψ is the azimuth of the absolute motion velocity projected onto the plane of the interferometer, with projected component v_P. Here the Fitzgerald-Lorentz contraction is a real dynamical effect of absolute motion, unlike the Einstein spacetime view that it is merely a spacetime perspective artifact, and whose magnitude depends on the choice of observer. The instrument is operated by rotating at a rate of one rotation over several minutes, and observing the shift in the fringe pattern through a telescope during the rotation. Then fringe shifts from six (Michelson and Morley) or twenty (Miller) successive rotations are averaged to improve the signal to noise ratio, and the average sidereal time noted.

9.3 Michelson-Morley Experiment 1887

Page 340 of the Michelson-Morley 1887 paper reporting the observed fringe shifts is reproduced in Fig.5. Each row of the table is the average from six successive rotations. In the graphs Michelson and Morley are noting that the fringe shifts are much smaller than expected. But they were using Newtonian physics to calibrate the device. We now know that the detector is nearly 2000 times less sensitive than given by that calibration, and that these fringe shifts correspond to a speed in excess of 300km/s. Michelson and Morley implicitly assumed the Newtonian value k=1, while Miller used an indirect method to estimate the value of k, as he understood that the Newtonian theory was invalid, but had no other theory for the interferometer. Of course the Einstein postulates, as distinct from Special Relativity, have that absolute motion has no meaning, and so effectively demands that $k = 0$. Using $k = 1$ gives only a nominal value for v_P, being some 8–9 km/s for the Michelson and Morley experiment, and some 10 km/s from Miller; the difference arising from the different latitudes of Cleveland and Mt. Wilson, and from Michelson and Morley taking data at limited times. So already Miller knew that his observations were consistent with those of Michelson and Morley, and so the important need for reproducibility was being confirmed.

means 0·02 wave-length. The rotation in the observations at noon was contrary to, and in the evening observations, with, that of the hands of a watch.

NOON OBSERVATIONS.

	16.	1.	2.	3.	4.	5.	6.	7.	8.	9.	10.	11.	12.	13.	14.	15.	16.
July 8.....	44·7	44·0	43·5	39·7	35·2	34·7	34·3	32·5	28·2	26·2	23·8	23·2	20·3	18·7	17·5	16·8	13·7
July 9.....	57·4	57·3	58·2	59·2	58·7	60·2	60·8	62·0	61·5	63·3	65·8	67·3	69·7	70·7	73·0	70·2	72·2
July 11.. ...	27·3	23·5	22·0	19·3	19·2	19·3	18·7	18·8	16·2	14·3	13·3	12·8	13·3	12·3	10·2	7·3	6·5
Mean.....	43·1	41·6	41·2	39·4	37·7	38·1	37·9	37·8	35·3	34·6	34·3	34·4	34·4	33·9	33·6	31·4	30·8
Mean in w. l.	·862	·832	·824	·788	·754	·762	·758	·756	·706	·692	·686	·688	·688	·678	·672	·628	·616
	·706	·692	·686	·688	·688	·678	·672	·628	·616								
Final mean.	·784	·762	·755	·738	·721	·720	·715	·692	·661								

P. M. OBSERVATIONS.

July 8... ...	61·2	63·3	63·3	68·2	67·7	69·3	70·3	69·8	69·0	71·3	71·3	70·5	71·2	71·2	70·5	72·5	75·7
July 9.....	26·0	26·0	28·2	29·2	31·5	32·0	31·3	31·7	33·0	35·8	36·5	37·3	38·8	41·0	42·7	43·7	44·0
July 12.....	66·8	66·5	66·0	64·3	62·2	61·0	61·3	59·7	58·2	55·7	53·7	54·7	55·0	58·2	58·5	57·0	56·0
Mean	51·3	51·9	52·5	53·9	53·8	54·1	54·3	53·7	53·4	54·3	53·8	54·2	55·0	56·8	57·2	57·7	58·6
Mean in w. l.	1·026	1·038	1·050	1·078	1·076	1·082	1·086	1·074	1·068	1·086	1·076	1·084	1·100	1·136	1·144	1·154	1·172
	1·068	1·086	1·076	1·084	1·100	1·136	1·144	1·154	1·172								
Final mean.	1·047	1·062	1·063	1·081	1·088	1·109	1·115	1·114	1·120								

The results of the observations are expressed graphically in fig. 6. The upper is the curve for the observations at noon, and the lower that for the evening observations. The dotted curves represent *one-eighth* of the theoretical displacements. It seems fair to conclude from the figure that if there is any dis-

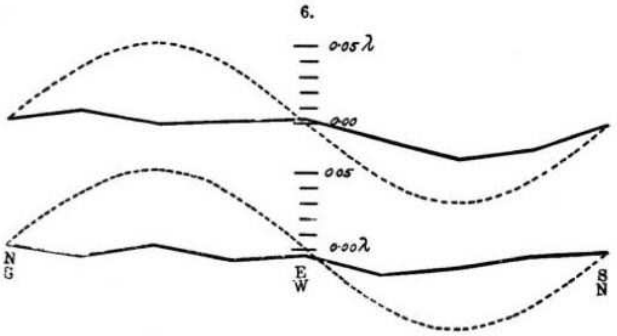

placement due to the relative motion of the earth and the luminiferous ether, this cannot be much greater than 0·01 of the distance between the fringes.

Considering the motion of the earth in its orbit only, this

Figure 5: Page 340 from the 1887 Michelson-Morley paper [2] showing the table of observed fringe shifts, measured here in divisions of the telescope screw thread, and which is analysed using (69) with the results shown in Fig.6.

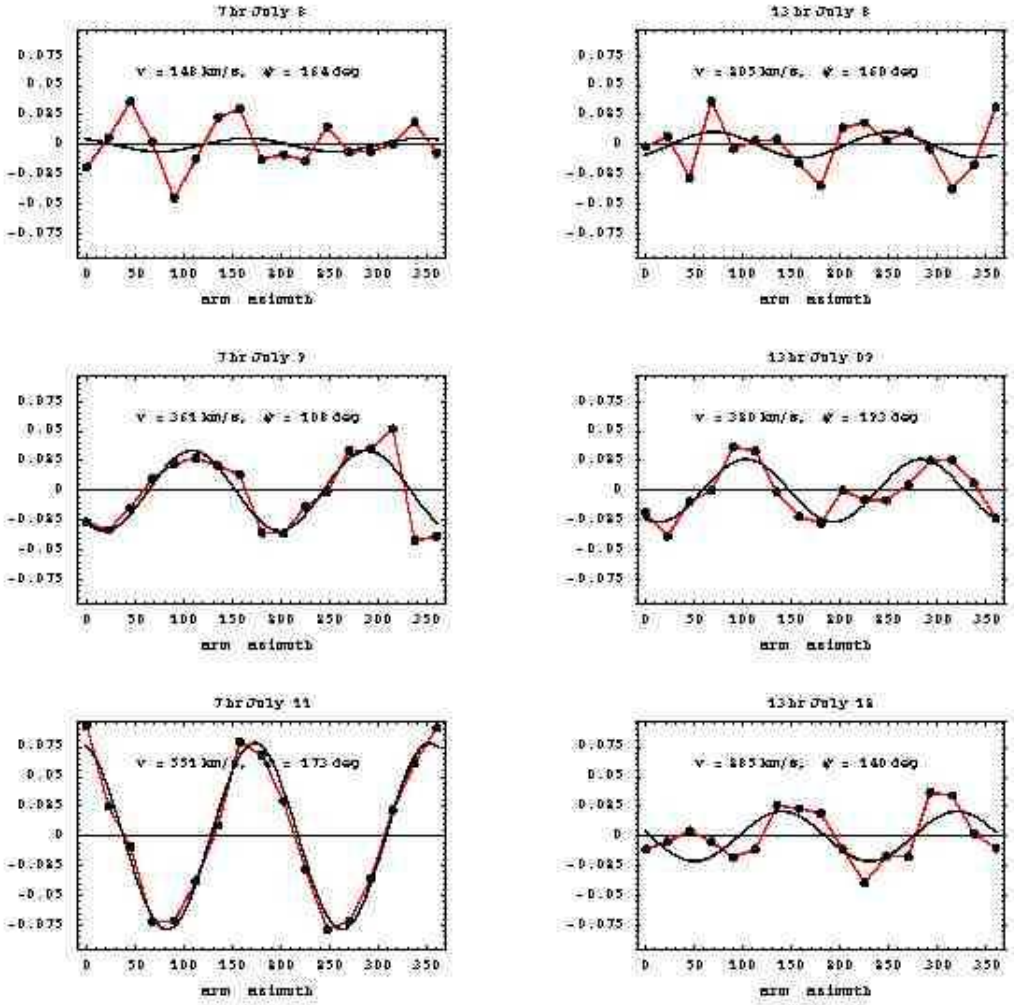

Figure 6: Analysis of the Michelson-Morley fringe shift data from the table in Fig.5. The plots are for the sidereal times and days indicated, and each plot arises from averaging six successive rotations, i.e. only 36 rotations were performed in July 1887. The data was fitted with (69) by a 6 parameter least-squares-fit by varying v_P, ψ, a, β, e and f. Only v_P and ψ are of physical interest, and are shown in each plot. ψ is measured clockwise from North. After these parameters have been determined the Hicks and temperature terms were subtracted from the data, and plotted above together with the $\cos\big(2(\theta-\psi)\big)$ expression. This makes the fringe shifts more easily seen. We see that four of the plots show a good fit to the expected form, while the other two give a poor fit. We also see that at the same time on successive days the speed and direction are significantly different. These are 'gravitational wave' effects, and were seen in later experiments as well.

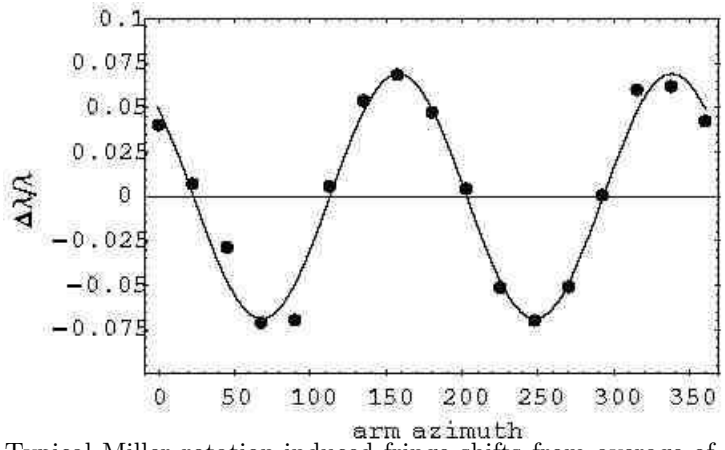

Figure 7: Typical Miller rotation-induced fringe shifts from average of 20 rotations, measured every 22.5°, in fractions of a wavelength $\Delta\lambda/\lambda$, vs arm azimuth θ(deg), measured clockwise from North, from Cleveland Sept. 29, 1929 16:24 UT; 11:29 hrs average local sidereal time. The curve is the best fit using the form in (69), and then subtracting the Hick's $\cos(\theta - \beta)$ and temperature terms from the data. Best fit gives $\psi = 158°$, or 22° measured from South, and a projected speed of $v_P = 315$ km/s. This plot shows the high quality of the Miller fringe shift observations. In the 1925/26 run of observations the rotations were repeated some 8,000 times.

9.4 Miller Experiment 1925/26

The Michelson and Morley air-mode interferometer fringe shift data was based upon a total of only 36 rotations in July 1887, revealing the nominal speed of some 8–9 km/s when analysed using the prevailing but incorrect Newtonian theory which has $k = 1$ in (69), and this value was known to Michelson and Morley. Including the Fitzgerald-Lorentz dynamical contraction effect as well as the effect of the gas present as in (69) we find that $n_{air} = 1.00029$ gives $k^2 = 0.00058$ for air, which explains why the observed fringe shifts were so small. They rejected their own data on the sole but spurious ground that the value of 8 km/s was smaller than the speed of the Earth about the Sun of 30km/s. What their result really showed was that (i) absolute motion had been detected because fringe shifts of the correct form, as in (69), had been detected, and (ii) that the theory giving $k^2 = 1$ was wrong, that Newtonian physics had failed. Michelson and Morley in 1887 should have announced that the speed of light did depend of the direction of travel, that the speed was relative to an actual physical 3-space. However contrary to their own data they concluded that absolute motion had not been detected. This has had enormous implications for fundamental theories of space

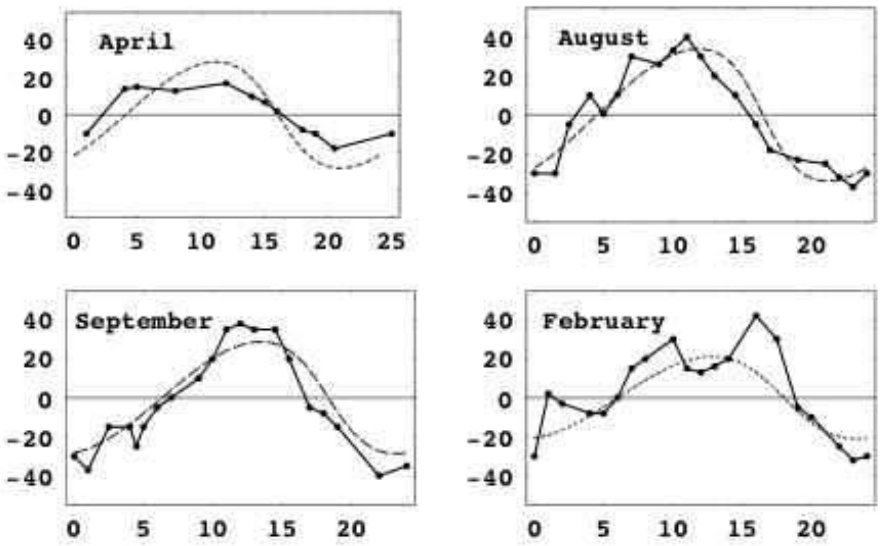

Figure 8: Miller azimuths ψ, measured from south and plotted against sidereal time in hrs, showing both data and best fit of theory giving $v = 433$ km/s in the direction $(\alpha = 5.2^{hr}, \delta = -67^0)$, using $n = 1.000226$ appropriate for the altitude of Mt. Wilson. The variation form month to month arises from the orbital motion of the earth about the sun: in different months the vector sum of the galactic velocity of the solar system with the orbital velocity and sun in-flow velocity is different. As shown in Fig.9 DeWitte using a completely different experiment detected the same direction and speed.

and time over the last 100 years.

It was Miller [3] who recognised that in the 1887 paper the theory for the Michelson interferometer must be wrong. To avoid using that theory Miller introduced the scaling factor k, even though he had no theory for its value. He then used the effect of the changing vector addition of the Earth's orbital velocity and the absolute galactic velocity of the solar system to determine the numerical value of k, because the orbital motion modulated the data, as shown in Fig.8. By making some 8,000 rotations of the interferometer at Mt. Wilson in 1925/26 Miller determined the first estimate for k and for the absolute linear velocity of the solar system. Fig.7 shows typical data from averaging the fringe shifts from 20 rotations of the Miller interferometer, performed over a short period of time, and clearly shows the expected form in (69). In Fig.7 the fringe shifts during rotation are given as fractions of a wavelength, $\Delta\lambda/\lambda = \Delta t/T$, where Δt is given by (69) and T is the period of the light. Such rotation-induced fringe shifts clearly

show that the speed of light is different in different directions. The claim that Michelson interferometers, operating in gas-mode, do not produce fringe shifts under rotation is clearly incorrect. But it is that claim that lead to the continuing belief, within physics, that absolute motion had never been detected, and that the speed of light is invariant. The value of ψ from such rotations together lead to plots like those in Fig.8, which show ψ from the 1925/1926 Miller [3] interferometer data for four different months of the year, from which the RA = 5.2 hr is readily apparent. While the orbital motion of the Earth about the Sun slightly affects the RA in each month, and Miller used this effect to determine the value of k, the new theory of gravity required a reanalysis of the data , revealing that the solar system has a large observed galactic velocity of some 420±30 km/s in the direction (RA = 5.2 hr, Dec = −67°). This is different from the speed of 369 km/s in the direction (RA = 11.20 hr, Dec = −7.22°) extracted from the Cosmic Microwave Background (CMB) anisotropy, and which describes a motion relative to the distant universe, but not relative to the local 3-space. The Miller velocity is explained by galactic gravitational in-flows [1].

An important implication of the new understanding of the Michelson interferometer is that vacuum-mode resonant cavity experiments should give a null effect, as is the case [26].

9.5 Other Gas-mode Michelson Interferometer Experiments

Two old interferometer experiments, by Illingworth [19] and Joos [20], used helium, enabling the refractive index effect to be recently confirmed, because for helium, with $n = = 1.000036$, we find that $k^2 = 0.00007$. Until the refractive index effect was taken into account the data from the helium-mode experiments appeared to be inconsistent with the data from the air-mode experiments; now they are seen to be consistent. Ironically helium was introduced in place of air to reduce any possible unwanted effects of a gas, but we now understand the essential role of the gas. The data from an interferometer experiment by Jaseja *et al.* [21], using two orthogonal masers with a He-Ne gas mixture, also indicates that they detected absolute motion, but were not aware of that as they used the incorrect Newtonian theory and so considered the fringe shifts to be too small to be real, reminiscent of the same mistake by Michelson and Morley. While the Michelson interferometer is a 2nd order device, as the effect of absolute motion is proportional to $(v/c)^2$, as in (69), but 1st order devices are also possible and the coaxial cable experiments described next are in this class.

9.6 Coaxial Cable Speed of EM Waves Anisotropy Experiments

Rather than use light travel time experiments to demonstrate the anisotropy of the speed of light, another technique is to measure the one-way speed of radio waves through a coaxial electrical cable. While this not a direct 'ideal' technique, as then the complexity of the propagation physics comes into play, it provides not only an independent confirmation of the light anisotropy effect, but also one which takes advantage of modern electronic timing technology.

9.7 Torr-Kolen Coaxial Cable Anisotropy Experiment

The first one-way coaxial cable speed-of-propagation experiment was performed at the Utah University in 1981 by Torr and Kolen. This involved two rubidium clocks placed approximately 500 m apart with a 5 MHz radio frequency (RF) signal propagating between the clocks via a buried EW nitrogen-filled coaxial cable maintained at a constant pressure of 2 psi. Torr and Kolen found that, while the round-trip speed time remained constant within $0.0001\%\, c$, as expected from Sect.7, variations in the one-way travel time were observed. The maximum effect occurred, typically, at the times predicted using the Miller galactic velocity, although Torr and Kolen appear to have been unaware of the Miller experiment. As well Torr and Kolen reported fluctuations in both the magnitude, from 1–3 ns, and the time of maximum variations in travel time. These effects are interpreted as arising from the turbulence in the flow of space past the Earth.

9.8 De Witte Coaxial Cable Anisotropy Experiment

During 1991 Roland De Witte performed a most extensive RF coaxial cable travel-time anisotropy experiment, accumulating data over 178 days. His data is in complete agreement with the Michelson-Morley 1887 and Miller 1925/26 interferometer experiments. The Miller and De Witte experiments will eventually be recognised as two of the most significant experiments in physics, for independently and using different experimental techniques they detected essentially the same velocity of absolute motion. But also they detected turbulence in the flow of space past the Earth — none other than gravitational waves. The De Witte experiment was within Belgacom, the Belgium telecommunications company. This organisation had two sets of atomic clocks in two buildings in Brussels separated by 1.5 km and the research project was an investigation of the task of synchronising these two clusters of atomic clocks. To that end 5MHz RF signals were

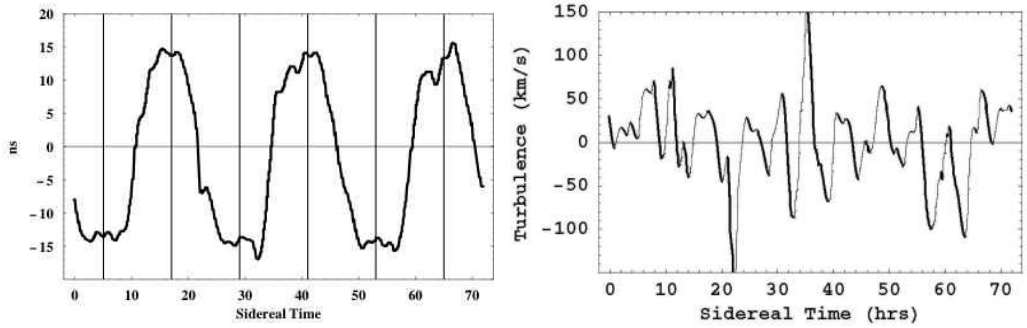

Figure 9: (a) Variations in twice the one-way travel time, in ns, for an RF signal to travel 1.5 km through a coaxial cable between Rue du Marais and Rue de la Paille, Brussels. An offset has been used such that the average is zero. The cable has a North-South orientation, and the data is ± difference of the travel times for NS and SN propagation. The sidereal time for maximum effect of ∼ 5 hr and ∼ 17 hr (indicated by vertical lines) agrees with the direction found by Miller. Plot shows data over 3 sidereal days and is plotted against sidereal time. The fluctuations are evidence of turbulence of gravitational waves. (b) Shows the speed fluctuations, essentially 'gravitational waves' observed by De Witte in 1991 from the measurement of variations in the RF coaxial-cable travel times. This data is obtained from that in (a) after removal of the dominant effect caused by the rotation of the Earth. Ideally the velocity fluctuations are three-dimensional, but the De Witte experiment had only one arm. This plot is suggestive of a fractal structure to the velocity field. This is confirmed by the power law analysis in [11, 23].

sent in both directions through two buried coaxial cables linking the two clusters. The atomic clocks were caesium beam atomic clocks, and there were three in each cluster: A1, A2 and A3 in one cluster, and B1, B2, and B3 at the other cluster. In that way the stability of the clocks could be established and monitored. One cluster was in a building on Rue du Marais and the second cluster was due south in a building on Rue de la Paille. Digital phase comparators were used to measure changes in times between clocks within the same cluster and also in the one-way propagation times of the RF signals. At both locations the comparison between local clocks, A1-A2 and A1-A3, and between B1-B2, B1-B3, yielded linear phase variations in agreement with the fact that the clocks have not exactly the same frequencies together with a short term and long term phase noise. But between distant clocks A1 toward B1 and B1 toward A1, in addition to the same linear phase variations, there is also an additional clear sinusoidal-like phase undulation with an approximate 24 hr period of the order of 28 ns peak to peak, as shown in Fig. 9. The experiment was performed over 178 days, making it possible to

measure with an accuracy of 25 s the period of the phase signal to be the sidereal day (23 hr 56 min).

Changes in propagation times were observed over 178 days from June 3 to November 27, 1991. A sample of the data, plotted against sidereal time for just three days, is shown in Fig.9. De Witte recognised that the data was evidence of absolute motion but he was unaware of the Miller experiment and did not realise that the Right Ascensions for minimum/maximum propagation time agreed almost exactly with that predicted using the Miller's direction (RA = 5.2 hr, Dec = −67°). In fact De Witte expected that the direction of absolute motion should have been in the CMB direction, but that would have given the data a totally different sidereal time signature, namely the times for maximum/minimum would have been shifted by 6 hrs. The declination of the velocity observed in this De Witte experiment cannot be determined from the data as only three days of data are available. The De Witte data is analysed in [24] and assuming a declination of 60° S a speed of 430 km/s is obtained, in good agreement with the Miller speed and Michelson-Morley speed. So a different and non-relativistic technique is confirming the results of these older experiments. This is dramatic.

De Witte reported the sidereal time of the 'zero' cross-over time, that is in Fig.9 for all 178 days of data. That showed that the time variations are correlated with sidereal time and not local solar time. A least-squares best fit of a linear relation to that data gives that the cross-over time is retarded, on average, by 3.92 minutes per solar day. This is to be compared with the fact that a sidereal day is 3.93 minutes shorter than a solar day. So the effect is certainly galactic and not associated with any daily thermal effects, which in any case would be very small as the cable is buried. Miller had also compared his data against sidereal time and established the same property, namely that the diurnal effects actually tracked sidereal time and not solar time, and that orbital effects were also apparent, with both effects apparent in Fig.8.

The dominant effect in Fig.9 is caused by the rotation of the Earth, namely that the orientation of the coaxial cable with respect to the average direction of the flow past the Earth changes as the Earth rotates. This effect may be approximately unfolded from the data leaving the gravitational waves shown in Fig.9, [11, 23]. This is the first evidence that the velocity field describing the flow of space has a complex structure, and is indeed fractal. The fractal structure, i. e. that there is an intrinsic lack of scale to these speed fluctuations, is demonstrated by binning the absolute speeds and counting the number of speeds within each bin, as discussed in [11, 23]. The Miller data also shows evidence of turbulence of the same magnitude. So far the data from four experiments, namely Miller, Torr

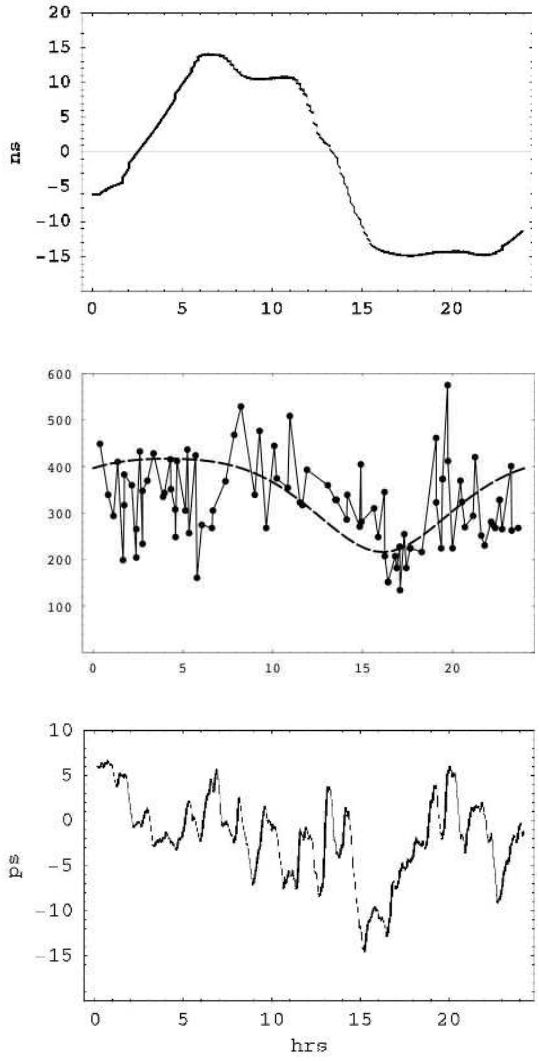

Figure 10: *Top:* De Witte data, with sign reversed, from the first sidereal day in Fig.9. This data gives a speed of approximately 430km/s. The data appears to have been averaged over more than 1hr, but still shows wave effects. *Middle:* Absolute projected speeds v_P in the Miller experiment plotted against sidereal time in hours for a composite day collected over a number of days in September 1925. Maximum projected speed is 417 km/s. The data shows considerable fluctuations. The dashed curve shows the non-fluctuating variation expected over one day as the Earth rotates, causing the projection onto the plane of the interferometer of the velocity of the average direction of the space flow to change. If the data was plotted against solar time the form is shifted by many hours. Note that the min/max occur at approximately 5 hrs and 17 hrs, as also seen by De Witte and in the Cahill experiment. *Bottom:* Data from the Cahill experiment [24] for one sidereal day on approximately August 23, 2006. We see similar variation with sidereal time, and also similar wave structure. This data has been averaged over a running 1hr time interval to more closely match the time resolution of the Miller experiment. These fluctuations are believed to be real wave phenomena of the 3-space. The new experiment gives a speed of 418 km/s. We see remarkable agreement between all three experiments.

and Kolen, De Witte and Cahill, show turbulence in the flow of space past the Earth. This is what can be called gravitational waves. This can be understood by noting that fluctuations in the velocity field induce ripples in the mathematical construct known as spacetime, as in (52). Such ripples in spacetime are known as gravitational waves.

9.9 Cahill Coaxial Cable Anisotropy Experiment

During 2006 Cahill [24] performed another RF coaxial cable anisotropy experiment. This detector uses a novel timing scheme that overcomes the limitations associated with the two previous coaxial cable experiments. The intention in such experiments is simply to measure the one-way travel time of RF waves propagating through the coaxial cable. To that end one would apparently require two very accurate clocks at each end, and associated RF generation and detection electronics. However the major limitation is that even the best atomic clocks are not sufficiently accurate over even a day to make such measurements to the required accuracy, unless the cables are of order of a kilometre or so in length, and then temperature control becomes a major problem. The issue is that the time variations are of the order of 25 ps per 10 meters of cable. To measure that requires time measurements accurate to, say, 1 ps. But atomic clocks have accuracies over one day of around 100 ps, implying that lengths of around 1 kilometre would be required, in order for the effect to well exceed timing errors. Even then the atomic clocks must be brought together every day to resynchronise them, or use De Witte's method of multiple atomic clocks. The new experiment is based on the notion that optical fibers respond differently to coaxial cable with respect to the speed of propagation of EM radiation. Some results are shown in Fig.10.

10 Experimental and Observational Phenomena II

10.1 Gravitational Phenomena

We have shown above that the dynamics of 3-space involves two constants: G and α. When generalising the Schrödinger and Dirac equations to take account of this 3-space we discovered that we arrive at an explanation for the phenomenon of gravity including the equivalence principle, as well as an explanation for the spacetime formalism. Here we explore various consequences of this new explanation

for gravity particularly those effects which reveal the effects of the α-dependent dynamics, in particular the bore hole anomaly which gives us the best estimate for the value of α from several bore hole experiments. The dynamical 3-space also gives a completely new account of black holes; an account completely different from the putative black holes of GR. In particular these new black holes generate an acceleration g that varies essentially as $1/r$, rather than as $1/r^2$ as in Newtonian gravity (NG) and GR. This is a dramatic difference. It explains immediately the rotation of spiral galaxies, for which the rotation speed is essentially constant at the outer limits, whereas NG and GR predict a $1/\sqrt{r}$ Keplerian form. It was this dramatic failure of NG and GR, and also in galactic clusters, that lead to the introduction of 'dark matter' - to generate a greater gravitational acceleration. The new theory of 3-space does not need this 'dark matter'. The black hole phenomena is complex, with minimal black holes induced by matter, to primordial black holes that attract matter. In the former case, and where the matter, in the form of stars and so on, has an essentially spherically symmetric distribution, it is possible to compute the effective mass of the induced minimal black holes. Observational data from these systems confirms the prediction. Other effects discussed are the gyroscope precession effect caused by the vorticity of the flow of 3-space past the earth. Finally we also discuss the cosmological Hubble expansion that arises from the 3-space dynamics. This gives an excellent parameter-free account of the redshift data from supernovae and gamma-ray bursts. GR requires 'dark energy' to fit that data, so here we see that the new 3-space dynamics does away with the need for 'dark energy'. Not discussed herein are anomalies in the Cavendish-like experiments to determine G [36], the gravitational lensing effects predicted by the generalised Maxwell equations, and also a re-analysis of the precession of elliptical orbits, particularly that of Mercury, and various other gravitational effects, see [1].

10.2 Bore Hole Anomaly and the Fine Structure Constant

We now show that the Airy method [32] originally proposed for measuring G actually gives a technique for determining the value of α from earth based bore hole gravity measurements. For a time-independent velocity field (7) may be written in the integral form

$$|\mathbf{v}(\mathbf{r})|^2 = 2G \int d^3r' \frac{\rho(\mathbf{r}') + \rho_{DM}(\mathbf{r}')}{|\mathbf{r} - \mathbf{r}'|}. \tag{70}$$

When the matter density of the earth is assumed to be spherically symmetric, and that the velocity field is now radial[6] (70) becomes

$$v(r)^2 = \frac{8\pi G}{r}\int_0^r s^2\left[\rho(s)+\rho_{DM}(s)\right]ds + 8\pi G\int_r^\infty s\left[\rho(s)+\rho_{DM}(s)\right]ds, \qquad (71)$$

where, with $v' = dv(r)/dr$,

$$\rho_{DM}(r) = \frac{\alpha}{8\pi G}\left(\frac{v^2}{2r^2}+\frac{vv'}{r}\right). \qquad (72)$$

Iterating (71) once we find to 1st order in α that

$$\rho_{DM}(r) = \frac{\alpha}{2r^2}\int_r^\infty s\rho(s)ds + O(\alpha^2), \qquad (73)$$

so that in spherical systems the 'dark matter' effect is concentrated near the centre, and we find that the total 'dark matter' is

$$M_{DM} \equiv 4\pi\int_0^\infty r^2\rho_{DM}(r)dr = \frac{4\pi\alpha}{2}\int_0^\infty r^2\rho(r)dr + O(\alpha^2) = \frac{\alpha}{2}M + O(\alpha^2) \quad (74)$$

where M is the total amount of (actual) matter. Hence to $O(\alpha)$ $M_{DM}/M = \alpha/2$ independently of the matter density profile. This turns out to be a very useful property as complete knowledge of the density profile is then not required in order to analyse observational data. As seen in Fig.11 the singular behaviour of both v and g means that there is a *black hole*[7] singularity at $r = 0$.

From (2), which is also the acceleration of matter [11], the gravity acceleration[8] is found to be, to 1st order in α, and using that $\rho(r) = 0$ for $r > R$, where R is the radius of the earth,

$$g(r) = \begin{cases} \dfrac{(1+\frac{\alpha}{2})GM}{r^2}, & r > R, \\ \dfrac{4\pi G}{r^2}\displaystyle\int_0^r s^2\rho(s)ds + \frac{2\pi\alpha G}{r^2}\int_0^r\left(\int_s^R s'\rho(s')ds'\right)ds, & r < R. \end{cases} \qquad (75)$$

This gives Newton's 'inverse square law' for $r > R$, even when $\alpha \neq 0$, which explains why the 3-space self-interaction dynamics did not overtly manifest in

[6]This in-flow is additional to the observed velocity of the earth through 3-space.

[7]These are called *black holes* because there is an event horizon, but in all other aspects differ from the *black holes* of General Relativity.

[8]We now use the convention that $g(r)$ is positive if it is radially inward.

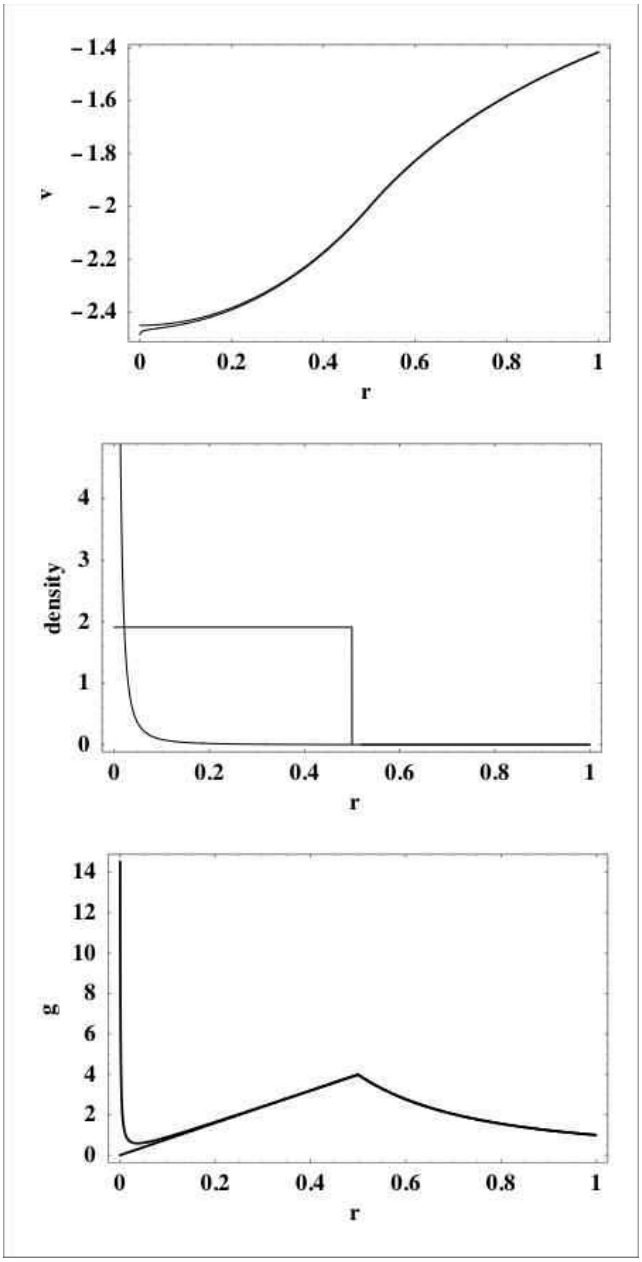

Figure 11: Upper plot shows speeds from numerical iterative solution of (71) for a solid sphere with uniform density and radius $r = 0.5$ for (i) upper curve the case $\alpha = 0$ corresponding to Newtonian gravity, and (ii) lower curve with $\alpha = 1/137$. These solutions ony differ significantly near $r = 0$. Middle plot shows matter density and 'dark matter' density ρ_{DM}, from (72), with arbitrary scales. Lower plot shows the acceleration from (2) for (i) the Newtonian in-flow from the upper plot, and (ii) from the $\alpha = 1/137$ case. The difference is only significant near $r = 0$. The accelerations begin to differ just inside the surface of the sphere at $r = 0.5$, according to (79). This difference is the origin of the bore hole g anomaly, and permits the determination of the value of α from observational data. This generic singular-g behaviour, at $r = 0$, is seen in the earth, in globular clusters and in galaxies.

the analysis of planetary orbits by Kepler and then Newton. However inside the earth (75) shows that $g(r)$ differs from the Newtonian theory, corresponding to $\alpha = 0$, as in Fig.11, and it is this effect that allows the determination of the value of α from the Airy method.

Expanding (75) in r about the surface, $r = R$, we obtain, to 1st order in α and for an arbitrary density profile, but not retaining any density gradients at the surface,

$$g(r) = \begin{cases} \dfrac{G_N M}{R^2} - \dfrac{2G_N M}{R^3}(r-R), & r > R, \\ \dfrac{G_N M}{R^2} - \left(\dfrac{2G_N M}{R^3} - 4\pi(1-\dfrac{\alpha}{2})G_N\rho\right)(r-R), & r < R \end{cases} \tag{76}$$

where ρ is the matter density at the surface, M is the total matter mass of the earth, and where we have defined

$$G_N \equiv (1+\frac{\alpha}{2})G. \tag{77}$$

The corresponding Newtonian gravity expression is obtained by taking the limit $\alpha \to 0$,

$$g_N(r) = \begin{cases} \dfrac{G_N M}{R^2} - \dfrac{2G_N M}{R^3}(r-R), & r > R, \\ \dfrac{G_N M}{R^2} - \left(\dfrac{2G_N M}{R^3} - 4\pi G_N\rho\right)(r-R), & r < R \end{cases} \tag{78}$$

Assuming Newtonian gravity (78) then means that from the measurement of difference between the above-ground and below-ground gravity gradients, namely $4\pi G_N\rho$, and also measurement of the matter density, permit the determination of G_N. This is the basis of the Airy method for determining G_N [32].

When analysing the bore hole data it has been found [33, 34] that the observed difference of the gravity gradients was inconsistent with $4\pi G_N\rho$ in (78), in that it was not given by the laboratory value of G_N and the measured matter density. This is known as the bore hole g anomaly and which attracted much interest in the 1980's. The bore hole data papers [33, 34] report the discrepancy, i.e. the anomaly or the gravity residual as it is called, between the Newtonian prediction and the measured below-earth gravity gradient. Taking the difference between (76) and (78), assuming the same unknown value of G_N in both, we obtain an expression for the gravity residual

$$\Delta g(r) \equiv g_N(r) - g(r) = \begin{cases} 0, & r > R, \\ 2\pi\alpha G_N\rho(r-R), & r < R. \end{cases} \tag{79}$$

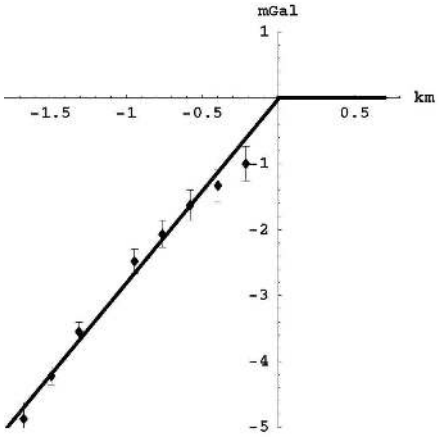

Figure 12: The data shows the gravity residuals for the Greenland Ice Shelf [33] Airy measurements of the $g(r)$ profile, defined as $\Delta g(r) = g_{Newton} - g_{observed}$, and measured in mGal (1mGal = 10^{-3} cm/s^2) and plotted against depth in km. The bore hole effect is that Newtonian gravity and the new theory differ only beneath the surface, provided that the measured above surface gravity gradient is used in both theories. This then gives the horizontal line above the surface. Using (79) we obtain $\alpha^{-1} = 137.9 \pm 5$ from fitting the slope of the data, as shown. The non-linearity in the data arises from modelling corrections for the gravity effects of the irregular sub ice-shelf rock topography.

When $\alpha \neq 0$ we have a two-parameter theory of gravity, and from (76) we see that measurement of the difference between the above ground and below ground gravity gradients is $4\pi(1-\frac{\alpha}{2})G_N\rho$, and this is not sufficient to determine both G_N and α, given ρ, and so the Airy method is now understood not to be a complete measurement by itself, i.e. we need to combine it with other measurements. If we now use laboratory Cavendish experiments to determine G_N, then from the bore hole gravity residuals we can determine the value of α, as already indicated in [37, 38]. These Cavendish experiments can only determine G_N up to corrections of order $\alpha/4$, simply because the analysis of the data from these experiments assumed the validity of Newtonian gravity [1]. So the analysis of the bore hole residuals will give the value of α up to $O(\alpha^2)$ corrections, which is consistent with the $O(\alpha)$ analysis reported above.

Gravity residuals from a bore hole into the Greenland Ice Shelf were determined down to a depth of 1.5 km by Ander *et al.* [33] in 1989. The observations were made at the Dye 3 2033 m deep bore hole, which reached the basement rock. This bore hole is 60 km south of the Arctic Circle and 125 km inland from the Greenland east coast at an elevation of 2530 m. It was believed that the ice provided an opportunity to use the Airy method to determine G_N, but now it is understood that in fact the bore hole residuals permit the determination of α, given a laboratory value for G_N. Various steps were taken to remove unwanted effects, such as imperfect knowledge of the ice density and, most dominantly,

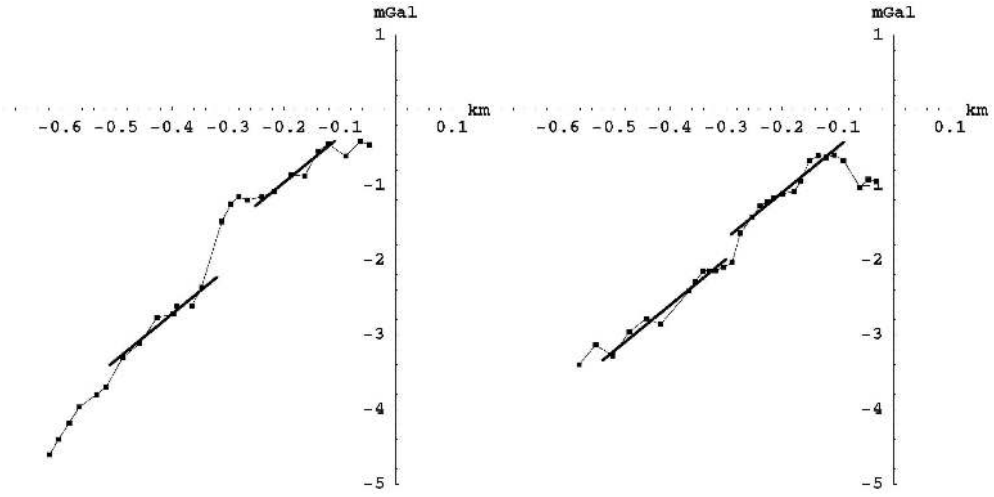

Figure 13: Gravity residuals from two of the Nevada bore hole experiments [34] that give a best fit of $\alpha^{-1} = 136.8 \pm 3$ on using (79). Some layering of the rock is evident.

the terrain effects which arises from ignorance of the profile and density inhomogeneities of the underlying rock. The bore hole gravity meter was calibrated by comparison with an absolute gravity meter. The ice density depends on pressure, temperature and air content, with the density rising to its average value of $\rho = 920$ kg/m^3 within some 200 m of the surface, due to compression of the trapped air bubbles. This surface gradient in the density has been modelled by the author, and is not large enough the affect the results. The leading source of uncertainty was from the gravitational effect of the bedrock topography, and this was corrected for using Newtonian gravity. The correction from this is actually the cause of the non-linearity of the data points in Fig.12. A complete analysis would require that the effect of this rock terrain be also computed using the new theory of gravity, but this was not done. Using $G_N = 6.6742 \times 10^{-11}$ m^{3}s^{-2}kg^{-1}, which is the current CODATA value, we obtain from a least-squares fit of the linear term in (79) to the data points in Fig.12 that $\alpha^{-1} = 137.9 \pm 5$, which equals the value of the fine structure constant $\alpha^{-1} = 137.036$ to within the errors, and for this reason we identify the constant α in (79) as being the fine structure constant. The first analysis [37, 38] of the Greenland Ice Shelf data incorrectly assumed that the ice density was 930 kg/m^3 which gave $\alpha^{-1} = 139 \pm 5$. However trapped air reduces the standard ice density to the ice shelf density of 920 kg/m^3, which brings the value of α immediately into better agreement with the value of

$\alpha = e^2/\hbar c$ known from quantum theory.

Thomas and Vogel [34] performed another bore hole experiment at the Nevada Test Site in 1989 in which they measured the gravity gradient as a function of depth, the local average matter density, and the above ground gradient, also known as the free-air gradient. Their intention was to test the extracted G_{local} and compare with other values of G_N, but of course using the Newtonian theory. The Nevada bore holes, with typically 3 m diameter, were drilled as a part of the U.S. Government tests of its nuclear weapons. The density of the rock is measured with a $\gamma - \gamma$ logging tool, which is essentially a γ-ray attenuation measurement, while in some holes the rock density was measured with a coreing tool. The rock density was found to be 2000 kg/m^3, and is dry. This is the density used in the analysis herein. The topography for 1 to 2 km beneath the surface is dominated by a series of overlapping horizontal lava flows and alluvial layers. Gravity residuals from two of the bore holes are shown in Figs.13. All gravity measurements were corrected for the earth's tide, the terrain on the surface out to 168 km distance, and the evacuation of the holes. The gravity residuals arise after allowing for, using Newtonian theory, the local lateral mass anomalies but assumed that the matter beneath the holes occurs in homogeneous ellipsoidal layers. We see in Fig.13 that the gravity residuals are linear with depth, where the density is the average value of 2000 kg/m^3, but interspersed by layers where the residuals show non-linear changes with depth. It is assumed here that these non-linear regions are caused by variable density layers. So in analysing this data we have only used the linear regions, and a simultaneous least-squares fit of the slope of (79) to the slopes of these four linear regions gives $\alpha^{-1} = 136.8 \pm 3$, which again is in extraordinary agreement with the value of 137.04 from quantum theory. Here we again used $G_N = 6.6742 \times 10^{-11}$ m^{3}s^{-2}kg^{-1}, as for the Greenland data analysis. Zumberge *et al.* [35] performed an extensive underwater Airy experiment, but failed to measure the above water g, so their results cannot be analysed in the above manner.

10.3 Black Hole Masses and the Fine Structure Constant

Equation (1) (with $\beta = -\alpha$) has 'black hole' solutions. The generic term 'black hole' is used because they have a compact closed event horizon where the inflow speed relative to the horizon equals the speed of light, but in other respects they differ from the putative black holes of General Relativity - in particular their gravitational acceleration is not inverse square law. The evidence is that it is these

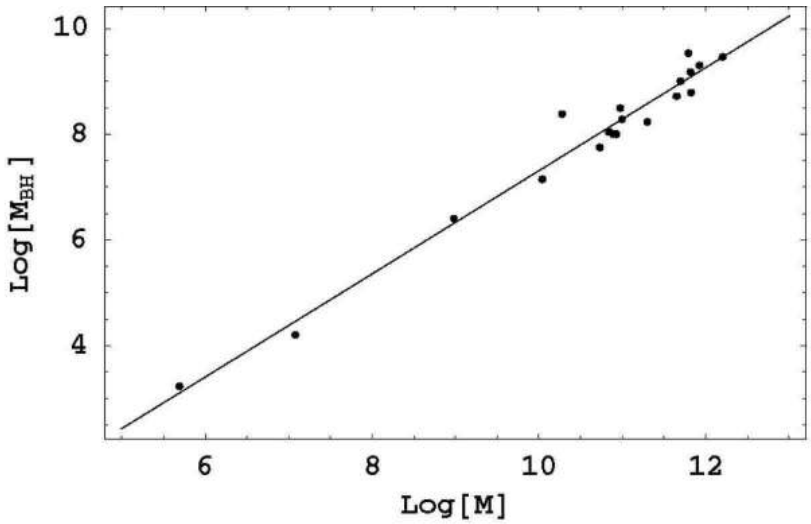

Figure 14: The data shows $\text{Log}_{10}[M_{BH}]$ for the black hole masses M_{BH} for a variety of spherical matter systems with masses M, plotted against $\text{Log}_{10}[M]$, in solar masses M_0. The straight line is the prediction from (81) with $\alpha = 1/137$. See [40] for references to the data.

new 'black holes' from (1) that have been detected. There are two categories: (i) an in-flow singularity induced by the flow into a matter system, such as, herein, a spherical galaxy or globular cluster. These black holes are termed minimal black holes, as their effective mass is minimal, (ii) primordial naked black holes which then attract matter. These result in spiral galaxies, and the effective mass of the black hole is larger than required merely by the matter induced in-flow. These are therefore termed non-minimal black holes. These explain the rapid formation of structure in the early universe, as the gravitational acceleration is approximately $1/r$ rather than $1/r^2$. This is the feature that also explains the so-called 'dark matter' effect in spiral galaxies. We consider now the minimal black holes.

Equation (1) has exact analytic 'black hole' solutions where $\rho = 0$ (actually a one-parameter family - but we write in this form for comparison with the next section)

$$v(r) = K\left(\frac{1}{r} + \frac{1}{R_s}\left(\frac{R_s}{r}\right)^{\frac{\alpha}{2}}\right)^{1/2} \tag{80}$$

where the $1/r$ term can only arise if matter is present, and the 2nd term is the 'black hole' effect. The consequent 'black hole' contribution to the total acceleration can be attributed to an effective mass M_{DM}, which we now also call

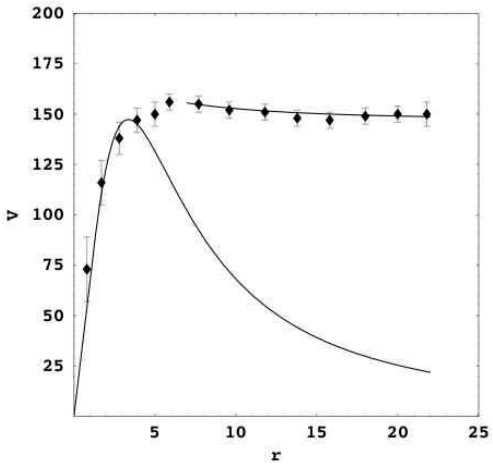

Figure 15: Data shows the non-Keplerian rotation-speed curve v_O for the spiral galaxy NGC 3198 in km/s plotted against radius in kpc/h. Lower curve is the rotation curve from the Newtonian theory for an exponential disk, which decreases asymptotically like $1/\sqrt{r}$. The upper curve shows the asymptotic form from (83), with the decrease determined by the small value of α. This asymptotic form is caused by the primordial black holes at the centres of spiral galaxies, and which play a critical role in their formation. The spiral structure is caused by the rapid in-fall towards these primordial black holes.

M_{BH}. To $O(\alpha)$ this effective mass is independent of the matter density profile, and is given by (74),

$$M_{BH} = M_{DM} = 4\pi \int_0^\infty r^2 \rho_{DM}(r) dr = \frac{\alpha}{2} M + O(\alpha^2) \tag{81}$$

This solution is applicable to the black holes at the centre of spherical star systems, where we identify M_{DM} as M_{BH}. So far black holes in 19 spherical star systems have been detected and together their masses are plotted in Fig.14 and compared with (81) [39, 40].

This result applies to any spherically symmetric matter distribution. This means that the bore hole anomaly is indicative of an in-flow singularity at the centre of the earth. This contributes some 0.4% of the effective mass of the earth, as defined by Newtonian gravity. However in star systems this minimal black hole effect is more apparent, and we label M_{DM} as M_{BH}. Essentially even in the non-relativistic regime the Newtonian theory of gravity, with its 'universal' Inverse Square Law, is deeply flawed.

10.4 Spiral Galaxies and the Rotation Anomaly

Equation (80) gives also a direct explanation for the spiral galaxy rotation anomaly. For a non-spherical system numerical solutions of (1) are required, but sufficiently far from the centre we find an exact non-perturbative two-parameter class of analytic solutions as in (80). There K and R_s are arbitrary constants in the $\rho = 0$

region, but whose values are determined by matching to the solution in the matter region. Here R_s characterises the length scale of the non-perturbative part of this expression, and K depends on α, G and details of the matter distribution. From (4) and (80) we obtain a replacement for the Newtonian 'inverse square law',

$$g(r) = \frac{K^2}{2}\left(\frac{1}{r^2} + \frac{\alpha}{2rR_s}\left(\frac{R_s}{r}\right)^{\frac{\alpha}{2}}\right), \tag{82}$$

in the asymptotic limit. The centripetal acceleration relation for circular orbits $v_O(r) = \sqrt{rg(r)}$ gives a 'universal rotation-speed curve'

$$v_O(r) = \frac{K}{2}\left(\frac{1}{r} + \frac{\alpha}{2R_s}\left(\frac{R_s}{r}\right)^{\frac{\alpha}{2}}\right)^{1/2} \tag{83}$$

Because of the α dependent part this rotation-velocity curve falls off extremely slowly with r, as is indeed observed for spiral galaxies. An example is shown in Fig.15. It was the inability of the Newtonian gravity and GR to explain these observations that led to the notion of 'dark matter'. So 'dark matter' is not a part of reality.

For the spatial flow in (80) we may compute the effective 'dark matter' density from (72)

$$\rho_{DM}(r) = \frac{(1-\alpha)\alpha}{16\pi G}\frac{K^2}{R_s^3}\left(\frac{R_s}{r}\right)^{2+\alpha/2} \tag{84}$$

We see the standard $1/r^2$ behaviour usually attributed to 'dark matter' in spiral galaxies. It should be noted that the Newtonian component of (80) does not contribute, and that $\rho_{DM}(\mathbf{r})$ is exactly zero in the limit $\alpha \to 0$. So supermassive black holes and the spiral galaxy rotation anomaly are all α-dynamics phenomena.

10.5 Lense-Thirring Effect and the GPB Gyroscope Experiment

The Gravity Probe B (GP-B) satellite experiment was launched in April 2004. It has the capacity to measure the precession of four on-board gyroscopes to unprecedented accuracy [42, 43, 44, 45]. Such a precession is predicted by GR, with two components (i) a geodetic precession, and (ii) a 'frame-dragging' precession known as the Lense-Thirring effect. The latter is particularly interesting effect

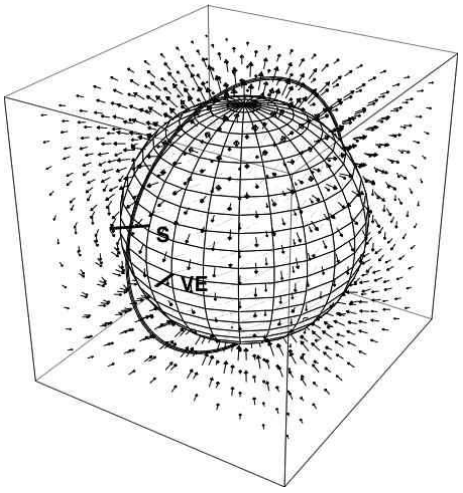

Figure 16: Shows the earth (N is up) and vorticity vector field component $\vec{\omega}$ induced by the rotation of the earth, as in (85). The polar orbit of the GP-B satellite is shown, **S** is the gyroscope starting spin orientation, directed towards the guide star IM Pegasi, RA = 22^h $53'$ $2.26''$, Dec = 16^0 $50'$ $28.2''$, and **VE** is the vernal equinox.

induced by the rotation of the earth, and described in GR in terms of a 'gravitomagnetic' field. According to GR this smaller effect will give a precession of 0.042 arcsec per year for the GP-B gyroscopes. Here we show that GR and the new theory make very different predictions for the 'frame-dragging' effect, and so the GP-B experiment will be able to decisively test both theories. While predicting the same earth-rotation induced precession, the new theory has an additional much larger 'frame-dragging' effect caused by the observed translational motion of the earth. As well the new theory explains the 'frame-dragging' effect in terms of vorticity in a 'substratum flow'. Herein the magnitude and signature of this new component of the gyroscope precession is predicted for comparison with data from GP-B when it becomes available.

Here we consider one difference between the two theories, namely that associated with the vorticity part of (12), leading to the 'frame-dragging' or Lense-Thirring effect. In GR the vorticity field is known as the 'gravitomagnetic' field $\mathbf{B} = -c\,\vec{\omega}$. In both GR and the new theory the vorticity is given by (10) but with a key difference: in GR $\mathbf{v}_R$ is *only* the rotational velocity of the matter in the earth, whereas in the 3-space dynamics $\mathbf{v}_R$ is the vector sum of the rotational velocity and the translational velocity of the earth through the substratum.

First consider the common but much smaller rotation induced 'frame-dragging' or vorticity effect. Then $\mathbf{v}_R(\mathbf{r}) = \mathbf{w} \times \mathbf{r}$ in (12), where $\mathbf{w}$ is the angular velocity of the earth, giving

$$\vec{\omega}(\mathbf{r}) = 4\frac{G}{c^2}\frac{3(\mathbf{r}.\mathbf{L})\mathbf{r} - r^2\mathbf{L}}{2r^5}, \tag{85}$$

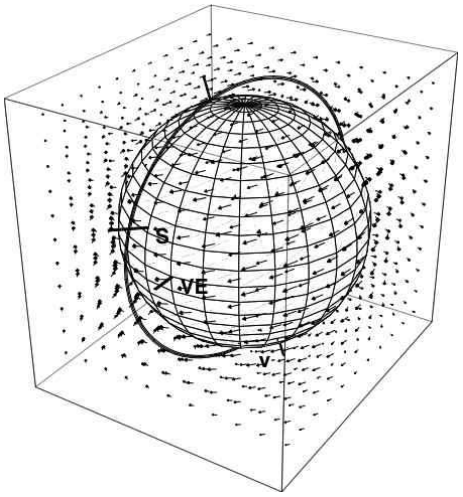

Figure 17: Shows the earth (N is up) and the much larger vorticity vector field component $\vec{\omega}$ induced by the translation of the earth, as in (88). The polar orbit of the GP-B satellite is shown, and **S** is the gyroscope starting spin orientation, directed towards the guide star IM Pegasi, RA = $22^h\ 53'\ 2.26''$, Dec = $16^0\ 50'\ 28.2''$, **VE** is the vernal equinox, and **V** is the direction RA = 5.2^h, Dec = -67^0 of the translational velocity $\mathbf{v}_c$.

where **L** is the angular momentum of the earth, and **r** is the distance from the centre. This component of the vorticity field is shown in Fig.16. Vorticity may be detected by observing the precession of the GP-B gyroscopes. The vorticity term in (85) leads to a torque on the angular momentum **S** of the gyroscope,

$$\vec{\tau} = \int d^3r\rho(\mathbf{r})\ \mathbf{r} \times (\vec{\omega}(\mathbf{r}) \times \mathbf{v}_R(\mathbf{r})), \tag{86}$$

where ρ is its density, and where $\mathbf{v}_R$ is used here to describe the rotation of the gyroscope. Then $d\mathbf{S} = \vec{\tau}dt$ is the change in **S** over the time interval dt. In the above case $\mathbf{v}_R(\mathbf{r}) = \mathbf{s} \times \mathbf{r}$, where **s** is the angular velocity of the gyroscope. This gives

$$\vec{\tau} = \frac{1}{2}\vec{\omega} \times \mathbf{S} \tag{87}$$

and so $\vec{\omega}/2$ is the instantaneous angular velocity of precession of the gyroscope. This corresponds to the well known fluid result that the vorticity vector is twice the angular velocity vector. For GP-B the direction of **S** has been chosen so that this precession is cumulative and, on averaging over an orbit, corresponds to some 7.7×10^{-6} arcsec per orbit, or 0.042 arcsec per year. GP-B has been superbly engineered so that measurements to a precision of 0.0005 arcsec are possible.

However for the unique translation-induced precession if we use $v_R \approx v_C =$ 430 km/s in the direction RA = 5.2^{hr}, Dec = -67^0, namely ignoring the effects of the orbital motion of the earth, the observed flow past the earth towards the sun, and the flow into the earth, and effects of the gravitational waves, then (12)

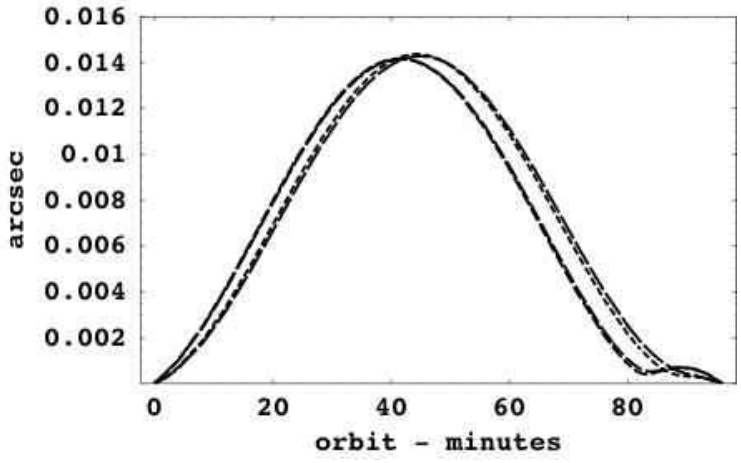

Figure 18: Predicted variation of the precession angle $\Delta\Theta = |\Delta\mathbf{S}(t)|/|\mathbf{S}(0)|$, in arcsec, over one 97 minute GP-B orbit, from the vorticity induced by the translation of the earth, as given by (89). The orbit time begins at location $\mathbf{S}$. Predictions are for the months of April, August, September and February, labeled by increasing dash length. The 'glitches' near 80 minutes are caused by the angle effects in (89). These changes arise from the effects of the changing orbital velocity of the earth about the sun. The GP-B expected angle measurement accuracy is 0.0005 arcsec.

gives

$$\vec{\omega}(\mathbf{r}) = \frac{2GM}{c^2}\frac{\mathbf{v}_C \times \mathbf{r}}{r^3}. \tag{88}$$

This much larger component of the vorticity field is shown in Fig.17. The maximum magnitude of the speed of this precession component is $\omega/2 = gv_C/c^2 = 8 \times 10^{-6}$arcsec/s, where here g is the gravitational acceleration at the altitude of the satellite. This precession has a different signature: it is not cumulative, and is detectable by its variation over each single orbit, as its orbital average is zero, to first approximation. Fig.18 shows $\Delta\Theta = |\Delta\mathbf{S}(t)|/|\mathbf{S}(0)|$ over one orbit, where, as in general,

$$\Delta\mathbf{S}(t) = \int_0^t dt' \frac{1}{2}\vec{\omega}(\mathbf{r}(t')) \times \mathbf{S}(t') \approx \left(\int_0^t dt' \frac{1}{2}\vec{\omega}(\mathbf{r}(t'))\right) \times \mathbf{S}(0). \tag{89}$$

Here $\Delta\mathbf{S}(t)$ is the integrated change in spin, and where the approximation arises because the change in $\mathbf{S}(t')$ on the RHS of (89) is negligible. The plot in Fig.18 shows this effect to be some 30× larger than the expected GP-B errors, and so easily detectable, if it exists as predicted herein. This precession is about the

instantaneous direction of the vorticity $\vec{\omega}(\mathbf{r}((t))$ at the location of the satellite, and so is neither in the plane, as for the geodetic precession, nor perpendicular to the plane of the orbit, as for the earth-rotation induced vorticity effect.

Because the yearly orbital rotation of the earth about the sun slightly effects $\mathbf{v}_C$ [16] predictions for four months throughout the year are shown in Fig.18. Such yearly effects were first seen in the Miller [3] experiment, see Fig.8.

10.6 Cosmology: Expanding 3-Space and the Hubble Effect

We now examine the predictions for the global expansion of the 3-space that follows from (1) (with $\beta = -\alpha$). We shall see that the solution gives an excellent parameter-free fit to the supernovae and gamma-ray bursts magnitude - redshift data [46]. This implies that there is no need to have a cosmological constant or 'dark energy', which are required by GR in order to fit this data. These also lead to the prediction that the universe expansion will accelerate in the future. This effect is also not required by the new 3-space dynamics. So, like 'dark matter', 'dark energy' is an unnecessary and spurious notion.

Suppose that we have a radially symmetric density $\rho(r,t)$ and that we look for a radially symmetric time-dependent flow $\mathbf{v}(\mathbf{r},t) = v(r,t)\hat{\mathbf{r}}$ from (1) (with $\beta = -\alpha$). Then $v(r,t)$ satisfies the equation, with $v' = \dfrac{\partial v(r,t)}{\partial r}$,

$$\frac{\partial}{\partial t}\left(\frac{2v}{r} + v'\right) + vv'' + 2\frac{vv'}{r} + (v')^2 + \frac{\alpha}{4}\left(\frac{v^2}{r^2} + \frac{2vv'}{r}\right) = -4\pi G\rho(r,t) \qquad (90)$$

Consider first the zero energy case $\rho = 0$. Then we have a Hubble solution $v(r,t) = H(t)r$, a centreless flow, determined by

$$\dot{H} + \left(1 + \frac{\alpha}{4}\right)H^2 = 0 \qquad (91)$$

with $\dot{H} = \dfrac{dH}{dt}$. We also introduce in the usual manner the scale factor $R(t)$ according to $H(t) = \dfrac{1}{R}\dfrac{dR}{dt}$. We then obtain the solution

$$H(t) = \frac{1}{(1+\frac{\alpha}{4})t} = H_0\frac{t_0}{t}; \quad R(t) = R_0\left(\frac{t}{t_0}\right)^{4/(4+\alpha)} \qquad (92)$$

where $H_0 = H(t_0)$ and $R_0 = R(t_0)$. We can write the Hubble function $H(t)$ in terms of $R(t)$ via the inverse function $t(R)$, i.e. $H(t(R))$ and finally as $H(z)$,

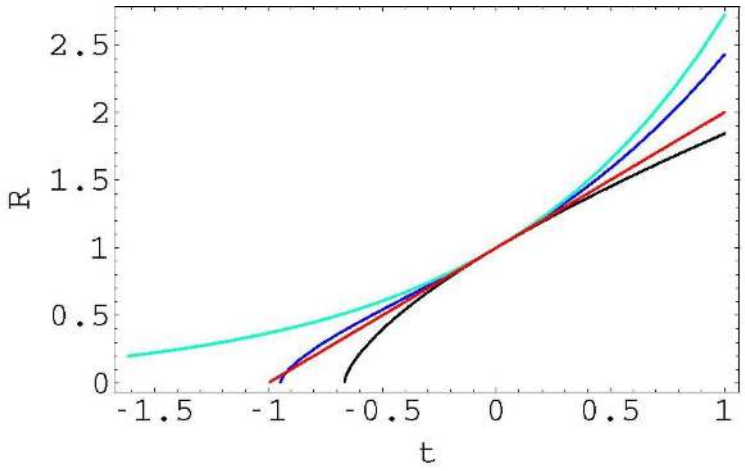

Figure 19: Plot of the scale factor $R(t)$ vs t, with $t = 0$ being 'now' with $R(0) = 1$, for the four cases discussed in the text, and corresponding to the plots in Figs.20 and 21: (i) the upper curve is the 'dark energy' only case, resulting in an exponential acceleration at all times, (ii) the bottom curve is the matter only prediction, (iii) the 2nd highest curve (to the right of $t = 0$) is the best-fit 'dark energy' plus matter case showing a past deceleration and future exponential acceleration effect. The straight line plot is the dynamical 3-space prediction showing a slightly older universe compared to case (iii). We see that the best-fit 'dark energy' - matter curve essentially converges on the dynamical 3-space result. All plots have the same slope at $t = 0$, i.e. the same value of H_0. If the age of the universe is inferred to be some 14Gyrs for case (iii) then the age of the universe is changed to some 14.7Gyr for case (iv).

where the redshift observed now, t_0, relative to the wavelengths at time t, is $z = R_0/R - 1$. Then we obtain

$$H(z) = H_0(1+z)^{1+\alpha/4} \tag{93}$$

We need to determine the distance travelled by the light from a supernova or gamma-ray burst (GRB) before detection, for this determines the apparent brightness. Using a choice of embedding-space coordinate system with $r = 0$ at the location of a supernova or GRB the speed of light relative to this embedding space frame is $c + v(r(t), t)$, i.e c wrt the space itself, as noted in Sect.5, where $r(t)$ is the distance from the source. Then the distance travelled by the light at time t after emission at time t_1 is determined implicitly by

$$r(t) = \int_{t_1}^{t} dt'(c + v(r(t'), t'), \tag{94}$$

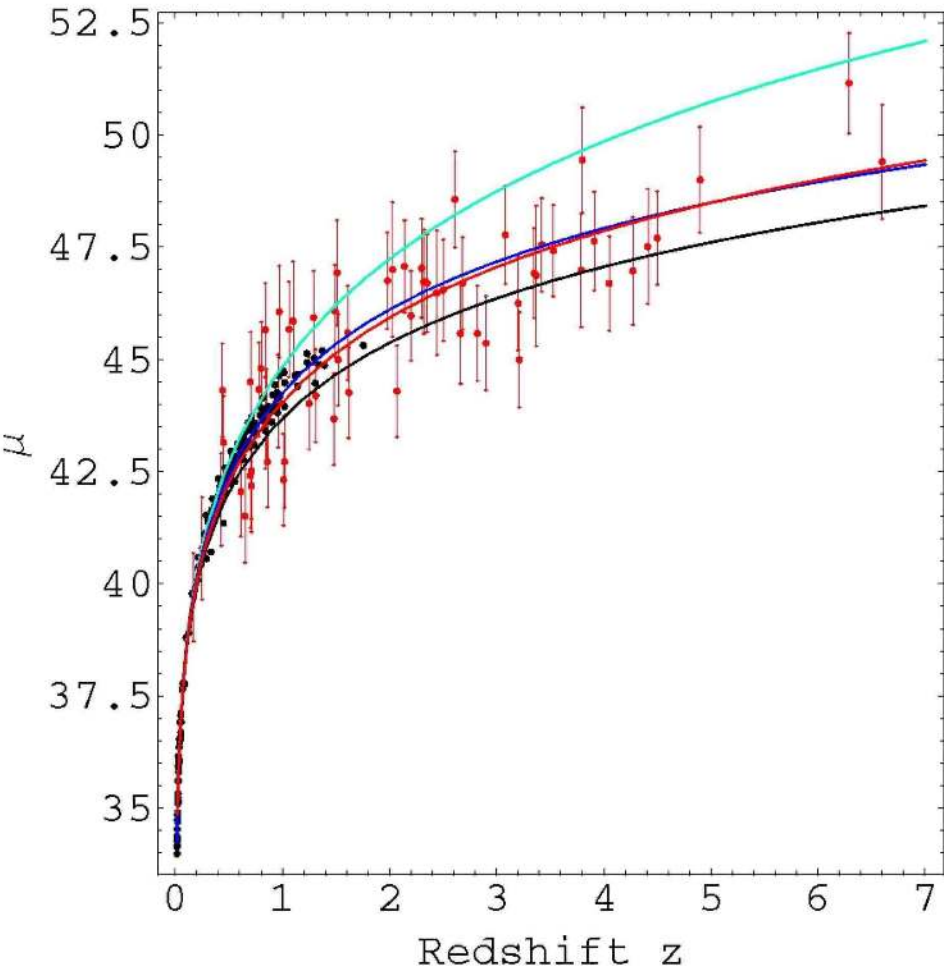

Figure 20: Hubble diagram showing the combined supernovae data from Davis *et al.* [47] using several data sets from Riess *et al.* (2007)[48] and Wood-Vassey *et al.* (2007)[49] (dots without error bars for clarity - see Fig.21 for error bars) and the Gamma-Ray Bursts data (with error bars) from Schaefer [50]. Upper curve (green) is 'dark energy' only $\Omega_\Lambda = 1$, lowest curve (black) is matter only $\Omega_m = 1$. Two middle curves show best fit of 'dark energy'-matter (blue) and dynamical 3-space prediction (red), and are essentially indistinguishable. However the theories make very different predictions for the future and for the age of the universe. We see that the best-fit 'dark energy' - matter curve essentially converges on the dynamical 3-space prediction.

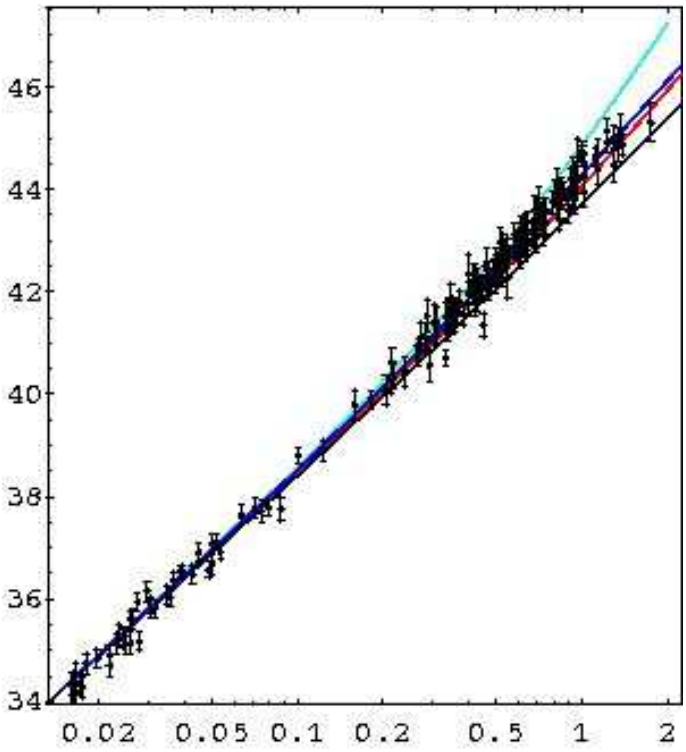

Figure 21: Hubble diagram as in Fig.20 but plotted logarithmically to reveal details for $z < 2$, and without GRB data. Upper curve (green) is 'dark energy' only $\Omega_\Lambda = 1$. Next curve (blue) is best fit of 'dark energy'-matter. Lowest curve (black) is matter only $\Omega_m = 1$. 2nd lowest curve (red) is dynamical 3-space prediction.

which has the solution, on using $v(r,t) = H(t)r$,

$$r(t) = cR(t) \int_{t_1}^{t} \frac{dt'}{R(t')} \tag{95}$$

Expressed in terms of the observable redshift z this gives

$$r(z) = c(1+z) \int_{0}^{z} \frac{dz'}{H(z')} \tag{96}$$

The effective dimensionless distance measure is given by

$$d(z) = (1+z) \int_{0}^{z} \frac{H_0 dz'}{H(z')} \tag{97}$$

and the theory distance modulus is then defined by

$$\mu_{th}(z) = 5 \log_{10}(d(z)) + m \tag{98}$$

Because all the selected supernova have the same absolute magnitude, the value of the constant m is determined by fitting the low z data. For the GRB data the magnitudes have been corrected so that the data gives a best fit to the dark energy/matter plot in Fig.20.

Using the Hubble expansion (93) in (97) and (98) we obtain the curve shown in Figs.20 and 21, yielding an excellent agreement with the supernovae and GRB data. Note that because $\alpha/4$ is so small it actually has negligible effect on these plots. Hence the dynamical 3-space gives an immediate account of the universe expansion data, and does not require the introduction of a cosmological constant or 'dark energy', but which will be nevertheless discussed next.

When the energy density is not zero we need to take account of the dependence of $\rho(r,t)$ on the scale factor of the universe. In the usual manner we thus write

$$\rho(r,t) = \frac{\rho_m}{R(t)^3} + \frac{\rho_r}{R(t)^4} + \Lambda \tag{99}$$

for matter, EM radiation and the cosmological constant or 'dark energy' Λ, respectively, where the matter and radiation is approximated by a spatially uniform (i.e independent of r) equivalent matter density. We argue here that Λ - the dark energy density, like dark matter, is an unnecessary concept. Then (90) becomes for $R(t)$

$$\frac{\ddot{R}}{R} + \frac{\alpha}{4}\frac{\dot{R}^2}{R^2} = -\frac{4\pi G}{3}\left(\frac{\rho_m}{R^3} + \frac{\rho_r}{R^4} + \Lambda\right) \tag{100}$$

giving

$$\dot{R}^2 = \frac{8\pi G}{3}\left(\frac{\rho_m}{R} + \frac{\rho_r}{R^2} + \Lambda R^2\right) - \frac{\alpha}{2}\int \frac{\dot{R}^2}{R} dR \tag{101}$$

In terms of $\dot{R}^2$ this has the solution

$$\dot{R}^2 = \frac{8\pi G}{3}\left(\frac{\rho_m}{(1-\frac{\alpha}{2})R} + \frac{\rho_r}{(1-\frac{\alpha}{4})R^2} + \frac{\Lambda R^2}{(1+\frac{\alpha}{4})} + bR^{-\alpha/2}\right) \tag{102}$$

which is easily checked by substitution into (101), and where b is an arbitrary integration constant. Finally we obtain from (102)

$$t(R) = \int_{R_0}^{R} \frac{dR}{\sqrt{\frac{8\pi G}{3}\left(\frac{\rho_m}{R} + \frac{\rho_r}{R^2} + \Lambda R^2 + bR^{-\alpha/2}\right)}} \tag{103}$$

where now we have re-scaled parameters $\rho_m \to \rho_m/(1-\frac{\alpha}{2}), \rho_r \to \rho_r/(1-\frac{\alpha}{4})$ and $\Lambda \to \Lambda/(1+\frac{\alpha}{4})$. When $\rho_m = \rho_r = \Lambda = 0$, (103) reproduces the expansion in

(92), and so the density terms in (103) give the modifications to the dominant purely spatial expansion dynamics, which we have noted above already gives an excellent account of the data. From (103) we then obtain

$$H(z)^2 = {H_0}^2(\Omega_m(1+z)^3 + \Omega_r(1+z)^4 + \Omega_\Lambda + \Omega_s(1+z)^{2+\alpha/2}) \tag{104}$$

with

$$\Omega_m + \Omega_r + \Omega_\Lambda + \Omega_s = 1. \tag{105}$$

Using the Hubble function (104) in (97) and (98) we obtain the plots in Figs.20 and 21 for four cases: (i) $\Omega_m = 0, \Omega_r = 0, \Omega_\Lambda = 1, \Omega_s = 0$, i.e a pure 'dark energy' driven expansion, (ii) $\Omega_m = 1, \Omega_r = 0, \Omega_\Lambda = 0, \Omega_s = 0$ showing that a matter only expansion is not a good account of the data, (iii) from a least squares fit with $\Omega_s = 0$ we find $\Omega_m = 0.28, \Omega_r = 0, \Omega_\Lambda = 0.68$ which led to the suggestion that 'dark energy' effect was needed to fix the poor fit from (ii), and finally (iv) $\Omega_m = 0, \Omega_r = 0, \Omega_\Lambda = 0, \Omega_s = 1$, as noted above, that the spatial expansion dynamics alone gives a good account of the data. Of course the EM radiation term Ω_r is non-zero but small and determines the expansion during the baryogenesis initial phase, as does the spatial dynamics expansion term because of the α dependence. If the age of the universe is inferred to be some 14Gyrs for case (iii) then, as seen in Fig.19, the age of the universe is changed to some 14.7Gyr for case (iv). We see that the best-fit 'dark energy' - matter curve essentially converges on the dynamical 3-space result.

The induced effective spacetime metric in (52) is for the Hubble expansion

$$ds^2 = g_{\mu\nu}dx^\mu dx^\nu = dt^2 - (d\mathbf{r} - H(t)\mathbf{r})dt)^2/c^2 \tag{106}$$

The occurrence of c has nothing to do with the dynamics of the 3-space - it is related to the geodesics of relativistic quantum matter, as shown in Sect.8. Changing variables $\mathbf{r} \to R(t)\mathbf{r}$ we obtain

$$ds^2 = g_{\mu\nu}dx^\mu dx^\nu = dt^2 - R(t)^2 d\mathbf{r}^2/c^2 \tag{107}$$

which is the usual Friedman-Robertson-Walker (FRW) metric in the case of a flat spatial section. However when solving for $R(t)$ using the Hilbert-Einstein GR equations the Ω_s term (with $\alpha \to 0$) is usually only present when the spatial curvature is non-zero. So some problem appears to be present in the usual GR analysis of the FRW metric. However above we see that that term arises in fact even when the embedding space is flat.

11 Conclusions

We have briefly reviewed the extensive evidence for a dynamical 3-space, with the minimal dynamical equation now known and confirmed by numerous experimental and observational data. This 3-space has been repeatedly detected since the Michelson-Morley experiment of 1887, and they also detected 'gravitational waves', which are just 3-space velocity fluctuations. As well the dynamical 3-space has been indirectly detected by means of the dynamical equation explaining diverse phenomena. We have shown that this equation has a Hubble expanding 3-space solution that in a parameter-free manner manifestly fits the recent supernovae and gamma-ray bursts redshift data. All of these successes imply that 'dark energy' and 'dark matter' are unnecessary notions. The Hubble solution leads to a uniformly expanding universe, and so without acceleration: the claimed acceleration is merely a spurious artifact related to the unnecessary 'dark energy' notion. This result gives an older age for the universe of some 14.7Gyr, and resolves as well various problems such as the fine turning problem, the horizon problem and other difficulties in the current modelling of the universe. We have also shown why the spacetime formalism appeared to be so successful, despite having no ontological status. One key discovery has been that Newton's theory of gravity is flawed, except in the very special case of planets in orbit about a sun, which is of course the restricted manifestation of gravity that was available to Newton.

At a deeper level the occurrence of α in (1) suggests that 3-space is actually a quantum system, and that (1) is merely a phenomenological description of that at the 'classical' level. In which case the α-dependent dynamics amounts to the detection of quantum space and quantum gravity effects, although clearly not of the form suggested by the quantisation of General Relativity. At a deeper level the information-theoretic *Process Physics* has given insights into the possible nature of reality as a limited self-referential system, in which quantum space and quantum matter are emergent phenomena, with both exhibiting non-local effects. In particular it implies that we have a 'universal' process time, as distinct from the current prevailing geometrical modelling of time. These results all suggest that a radically different paradigm for reality is emerging, and in which we see a unification of quantum space and quantum matter, and with gravity an emergent phenomenon.

Special thanks to Tim Eastman, Erich Weigold, Igor Bray and Lance McCarthy.

References

[1] Cahill R.T. *Process Physics: From Information Theory to Quantum Space and Matter*, Nova Science Pub., New York, 2005.

[2] Michelson A.A. and Morley E.W. *Philos. Mag.* S.5 24 No.151, 449-463, 1887.

[3] Miller D.C. *Rev. Mod. Phys.*, **5**, 203-242, 1933.

[4] Cahill R.T. *Process Physics*, *Process Studies Supplement*, Issue 5, 1-131, 2003.

[5] Cahill R.T. and Klinger C.M. *Bootstrap Universe from Self-referential Noise*, *Progress in Physics*, **2**, 108-112, 2005.

[6] Cahill R.T. and Klinger C.M. *Self-referential Noise as a Fundamental Aspect of Reality*, published in proc. *2nd Intl. Conf. on Unsolved Problems of Noise and Fluctuations (UPoN 99)*, eds Abbott, D. and Kish L. **511**, 43, *American Institute of Physics*, NY, 2000.

[7] Cahill R.T., Klinger C.M. and Kitto K. *Process Physics: Modelling Reality as Self-organising Information*, *The Physicist*, **37**(6), 191-195, 2000.

[8] Cahill R.T. and Klinger C.M. *Self-referential Noise and the Synthesis of Three-dimensional Space*, *Gen. Rel. and Grav.* **32**(3), 529, 2000.

[9] Cahill R.T. *Process Physics: Inertia, Gravity and the Quantum*, *Gen. Rel. and Grav.* **34**, 1637-1656, 2002.

[10] Newton I. *Philosophiae Naturalis Principia Mathematica*, 1687.

[11] Cahill R.T. *Dynamical Fractal 3-Space and the Generalised Schrödinger Equation: Equivalence Principle and Vorticity Effects*, *Progress in Physics*, **1**, 27-34, 2006.

[12] Ehrenfest P. *Z. Physik*, v.45, 455, 1927.

[13] Shnoll, S.E. *et al. Experiments with Radioactive Decay of* ^{239}Pu*: Evidence Sharp Anisotropy of Space*, *Progress in Physics*, v.1, pp.81-84, 2005, and references therein.

[14] Hertz H. *On the Fundamental Equations of Electro-Magnetics for Bodies in Motion*, *Wiedemann's Ann.* **41**, 369, 1890; *Electric Waves, Collection of Scientific Papers, Dover Pub.*, New York, 1962.

[15] Cahill R.T. *Dynamical 3-Space: Alternative Explanation of the 'Dark Matter Ring'*, arXiv:0705.2846v1, 2007.

[16] Cahill R.T. *Absolute Motion and Gravitational Effects*, *Apeiron*, **11**(1), 53-111, 2004.

[17] Cahill R.T. and Kitto K. *Michelson-Morley Experiments Revisited*, *Apeiron*, **10**(2),104-117, 2003.

[18] Cahill R.T. *The Michelson and Morley 1887 Experiment and the Discovery of Absolute Motion*, *Progress in Physics*, **3**, 25-29, 2005.

[19] Illingworth K.K. *Phys. Rev.* 3, 692-696, 1927.

[20] Joos G. *Ann. d. Physik* [5] 7, 385, 1930.

[21] Jaseja T.S. *et al. Phys. Rev.* A 133, 1221, 1964.

[22] Torr D.G. and Kolen P. in *Precision Measurements and Fundamental Constants*, Taylor, B.N. and Phillips, W.D. eds. *Natl. Bur. Stand. (U.S.), Spec. Pub.*, 617, 675, 1984.

[23] Cahill R.T. *The Roland DeWitte 1991 Experiment*, *Progress in Physics*, **3**, 60-65, 2006.

[24] Cahill R.T. *A New Light-Speed Anisotropy Experiment: Absolute Motion and Gravitational Waves Detected*, *Progress in Physics*, **4**, 73-92, 2006.

[25] Hicks W. M. *On the Michelson-Morley Experiment Relating to the Drift of the Ether. Phil. Mag.*, v. 3, 9–42, 1902.

[26] Müller, H. *et al. Modern Michelson-Morley Experiment using Cryogenic Optical Resonators. Phys. Rev. Lett.* 91(2), 020401-1, 2003.

[27] Cahill R.T. *The Michelson and Morley 1887 Experiment and the Discovery of 3-Space and Absolute Motion*, *Australian Physics*, **46**, 196-202, Jan/Feb 2006.

[28] Cahill R.T. *The Speed of Light and the Einstein Legacy: 1905-2005*, *Infinite Energy*, **10**(60), 28-27, 2005.

[29] Cahill R.T. *The Einstein Postulates 1905-2005: A Critical Review of the Evidence*, in *Einstein and Poincaré: The Physical Vacuum*, 129-141, ed V. Dvoeglazov, Apeiron, Montreal 2006.

[30] Levy J. *From Galileo to Lorentz...and Beyond*, Apeiron, Montreal, 2003.

[31] Guerra V. and de Abreu R. *Relativity Einstein's Lost Frame*, Extra]muros, 2005.

[32] Airy G.B. *Philos. Trans. R. Soc. London*, **146**, 297; v.146, 343, 1856.

[33] Ander M.E. *et al. Test of Newton's Inverse-Square Law in the Greenland Ice Cap*, *Phys. Rev. Lett.*, **62**, 985-988, 1989.

[34] Thomas J. and Vogel P. *Testing the Inverse-Square Law of Gravity in Bore Holes at the Nevada Test Site*, *Phys. Rev. Lett.*, **65**, 1173-1176, 1990.

[35] Zumberge M.A. *et al. Submarine Measurement of the Newtonian Gravitational Constant*, *Phys. Rev. Lett.*, **67**, 3051-3054, 1991.

[36] Cavendish H. *Philosophical Transactions*, 1798.

[37] Cahill R.T. *Gravity, 'Dark Matter' and the Fine Structure Constant*, *Apeiron*, **12**(2), 144-177, 2005.

[38] Cahill R.T. *'Dark Matter' as a Quantum Foam In-flow Effect*, in *Trends in Dark Matter Research*, 96-140, ed. J. Val Blain , Nova Science Pub., New York, 2005.

[39] Cahill R.T. *Black Holes in Elliptical and Spiral Galaxies and in Globular Clusters*, *Progress in Physics*, **3**, 51-56, 2005.

[40] Cahill R.T. *Black Holes and Quantum Theory: The Fine Structure Constant Connection*, *Progress in Physics*, **4**, 44-50, 2006.

[41] Lense J. and Thirring H. *Phys. Z.*, v.29, 156, 1918.

[42] L.I. Schiff, *Phys. Rev. Lett.* **4**, 215, 1960.

[43] R.A. Van Patten and C.W.F. Everitt, *Phys. Rev. Lett.* **36**, 629, 1976.

[44] C.W.F. Everitt *et al.*, in: *Near Zero: Festschrift for William M. Fairbank*, ed. C.W.F. Everitt, Freeman Ed,. S. Francisco, 1986.

[45] Cahill R.T. *Novel Gravity Probe B Frame-Dragging Effect*, *Progress in Physics*, **3**, 30-33, 2005.

[46] Cahill R.T. *Dynamical 3-Space: Supernova and the Hubble Expansion - Older Universe and End of Dark Energy*, arXiv:0705.1569v1, 2007.

[47] Davis T., Mortsell E., Sollerman J. and ESSENCE, *Scrutinizing Exotic Cosmological Models Using ESSENCE Supernova Data Combined with Other Cosmological Probes*, astro-ph/0701510, 2007.

[48] Riess A.G. *et al.*, *New Hubble Space Telescope Discoveries of Type Ia Supernovae at* $z > 1$*: Narrowing Constraints on the Early Behavior of Dark Energy*, astro-ph/0611572, 2007.

[49] Wood-Vassey W.M. *et al.*, *Observational Constraints on the Nature of the Dark Energy: First Cosmological Results from the ESSENCE Supernova Survey*, astro-ph/0701041, 2007.

[50] Schaefer B.E. *The Hubble Diagram to Redshift* > 6 *from 69 Gamma-Ray Bursts*, *Ap. J.* **660**, 16-46, 2007.